On the relationship between extension and anisotropy: Constraints from shear wave splitting across the East African Plateau

Kristoffer T. Walker,[1,2] Andrew A. Nyblade,[3] Simon L. Klemperer,[1]
Götz H. R. Bokelmann,[1,4] and Thomas J. Owens[5]

Received 28 October 2003; revised 2 April 2004; accepted 21 May 2004; published 6 August 2004.

[1] East Africa is a tectonically complex region owing to the presence of a rigid craton, paleothrust belts and shear zones, active magmatism and rifting, and possibly even a mantle plume. We present new splitting results of teleseismic shear phases recorded by 21 broadband seismic stations in Tanzania, seven broadband stations in Kenya, and three permanent broadband Global Seismic Network stations in Kenya and Uganda. Inconsistent apparent splitting is observed beneath the craton and along its southern and southeastern flank in Tanzania. Splitting at stations elsewhere in the rifts and orogenic belts is more consistent. We test between different models of anisotropy for stations with inconsistent splitting (single layer with horizontal fast axis, single layer with dipping fast axis, and two layers with horizontal fast axes). However, we show that these more complicated models do not reasonably explain the data. The data are explained better by a laterally (and/or in some places vertically) varying single-layer model with a horizontal fast axis. We arrive at a conceptual model of anisotropy in Tanzania and Kenya that is controlled by (1) active shear along the base of the plate associated with asthenospheric flow beneath and around the moving craton keel, (2) asthenospheric flow from a plume north of central Kenya, (3) fossilized anisotropy in the lithosphere due to past orogenic events, and possibly (4) aligned magma-filled lenses beneath the rifts. Our most robust conclusion is that we can rule out an extension-induced lattice preferred orientation of olivine as a dominant factor, which is surprising given the long history of extension in the region. This indicates that mantle-lithospheric extension in East Africa occurs via dikeintrusion and/or ductile thinning within narrow rift zones and is possibly facilitated by a mechanical lithospheric anisotropy imparted by fossilized north/south structural or mineralogical fabrics. *INDEX TERMS:* 7203 Seismology: Body wave propagation; 7218 Seismology: Lithosphere and upper mantle; 8109 Tectonophysics: Continental tectonics—extensional (0905); 8120 Tectonophysics: Dynamics of lithosphere and mantle—general; 8121 Tectonophysics: Dynamics, convection currents and mantle plumes; *KEYWORDS:* anisotropy, shear wave splitting, extension

Citation: Walker, K. T., A. A. Nyblade, S. L. Klemperer, G. H. R. Bokelmann, and T. J. Owens (2004), On the relationship between extension and anisotropy: Constraints from shear wave splitting across the East African Plateau, *J. Geophys. Res.*, *109*, B08302, doi:10.1029/2003JB002866.

1. Introduction

[2] The East African Plateau, covering some 1.8 × 10^6 km^2, is a well-recognized topographic and tectonic feature of the African Plate [*Nyblade and Robinson*, 1994] (Figure 1). The plateau has a mean elevation of about 1100 m and consists of Precambrian terranes including the Archean Tanzania craton in the center of the plateau and surrounding Proterozoic orogenic belts. Cenozoic extension is accommodated by rifting within the flanking orogenic belts, associated with widespread volcanism and low seismicity in the Eastern Rift and isolated volcanism and high seismicity in the Western Rift.

[3] Mechanisms and structures controlling the tectonics and geodynamics in East Africa remain unresolved in large part because few details are known about the nature of the upper mantle across east Africa. In addition, a number of hypotheses have been proposed to explain the origin of anisotropy beneath rifts, within cratons, and around hotspots. In this paper, we analyze and model splitting of teleseismic waveforms recorded by broadband seismic stations in Tanzania, Kenya, and Uganda, and we develop new constraints on the origin of anisotropy and more

[1]Department of Geophysics, Stanford University, Stanford, California, USA.
[2]Now at the Institute of Geophysics and Planetary Physics, Scripps Institution of Oceanography, University of California, San Diego, California, USA.
[3]Department of Geosciences, Pennsylvania State University, College Park, Pennsylvania, USA.
[4]Now at Laboratoire de Tectonophysique, Université de Montpellier II, Montpellier, France.
[5]Department of Geological Sciences, University of South Carolina, Columbia, South Carolina, USA.

0148-0227/04/2003JB002866$09.00

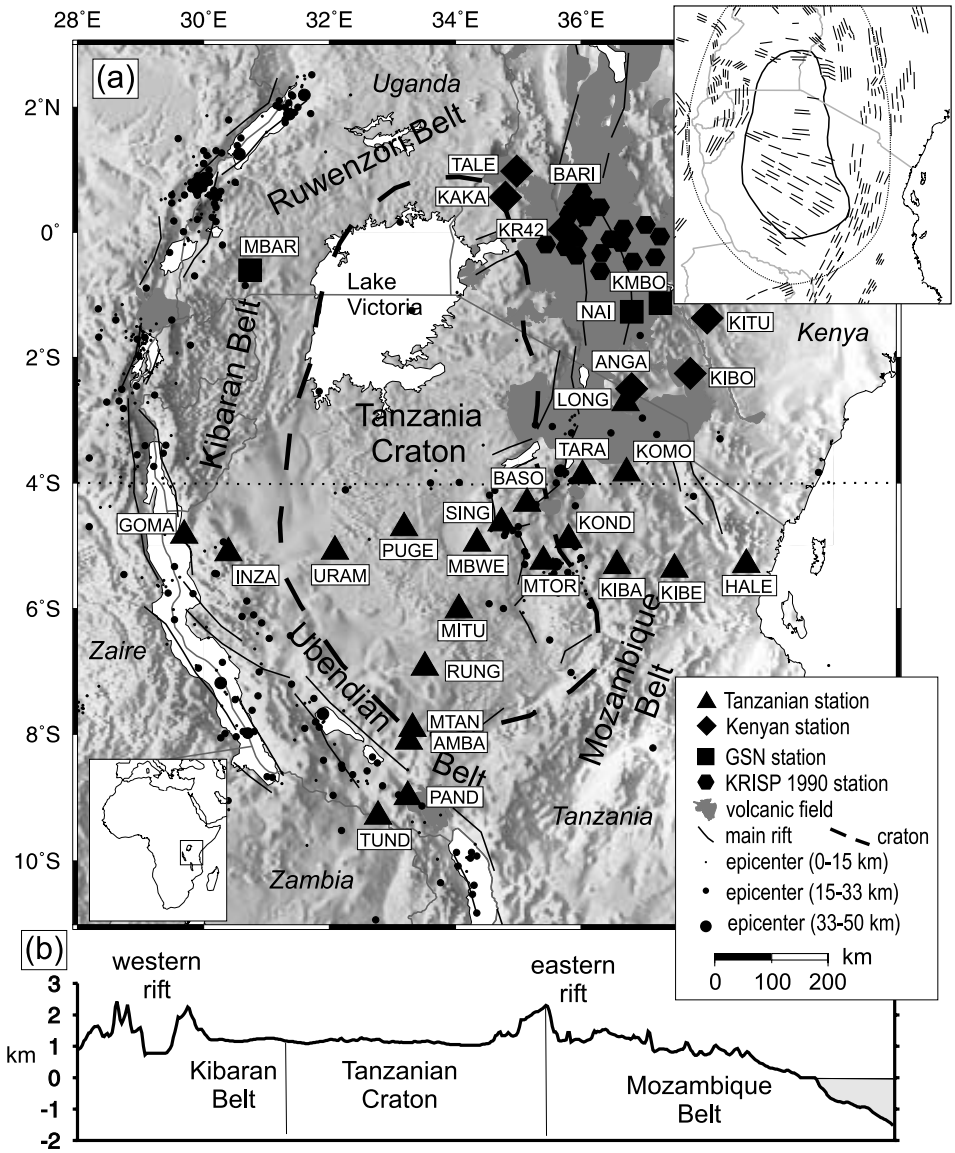

Figure 1. Topographic and structural map of East Africa. (a) Broadband three-component station locations of the 1994–1995 Tanzania Network, 1999–2002 Kenya Network, Global Seismic Network (GSN) stations (KMBO, MBAR, and NAI), and Kenya Rift International Seismic Project (KRISP) 1990 Network [*Gao et al.*, 1997]. The inset map in the upper right corner shows the general Precambrian structural trends in the mobile belts and craton [*Holmes*, 1951; *Cahen et al.*, 1984; *Shackleton*, 1986] (see also Figure 8) and the approximate boundaries of the East African Plateau (dotted line). (b) Topographic profile across 4°S (dotted line in Figure 1a) delineates the smooth topography across the elevated Tanzania craton. Surrounding the craton is highly irregular topography associated with the deforming rifts and old orogenic belts. Seismicity is taken from the Advanced National Seismic System database for years 1965–2003 with $M > 3.1$.

fundamentally, the relationship between tectonics, magmatism, and geodynamics beneath the East African Plateau.

1.1. Geology and Tectonic History

[4] The Tanzania craton is divided into two belts at 4.5°S: Nyzanian to the north and Dodoman to the south. The Dodoman consists mainly of quartzites, schists, amphibolites, and gneisses. The younger Nyzanian belt is composed of less deformed granite and greenstone belts. The youngest dates for the craton (~2500 Myr ago) come from granitic rocks near its eastern margin [*Cahen et al.*, 1984]. Major folds with consistent ESE/WNW fold axes are thought to have developed during the Early Archaen Dodoman and Nyzanian orogenies [*Holmes*, 1951; *Cahen et al.*, 1984; *Shackleton*, 1986].

[5] The Tanzania craton is bordered to the south and southwest by the Paleoproterozoic Ubendian Belt, a southeast striking strike-slip shear belt of granulites and amphibolites deformed during the Ubendian orogeny (2100–2025 Myr ago) [*Lenoir et al.*, 1994; *Theunissen et*

al., 1996]. The northern part of the Ubendian Belt is truncated west of the Tanzania craton by the NE trending Mesoproterozoic Kibaran Belt, and to the north of the craton lies the Paleoproterozoic Ruwenzori Belt [*Cahen et al.*, 1984]. To the east of the Tanzania craton lies the Neoproterozoic Mozambique Belt (Figure 1), which has N–NE striking structures formed by multiple collisional events 450–1200 Myr ago [*Cahen et al.*, 1984; *Shackleton*, 1986; *Key et al.*, 1989].

[6] The orogenic belts have been disrupted by extensional tectonism at least three times during the Phanerozoic [e.g., *Noble et al.*, 1997]. The first phase of rifting occurred along the modern East African coast during the Karoo (Permian-Jurassic) when Madagascar separated from Africa. In the Cretaceous a SE trending branch of the Central African rift system formed, extending from southern Sudan to the Kenya coast. The extensive East African rift (EAR) system formed later in the Cenozoic. The modern rift system is ~4000 km long and is characterized by two branches that surround the Tanzania craton, the Western Rift and the Eastern Rift (Figure 1). In Kenya, extension within the Eastern Rift has led to the formation of a narrow (50–80 km wide) graben commonly referred to as the Kenya Rift. In northeastern Tanzania, extension is accommodated by a diffuse zone (~300 km wide) of block faulting [*Dawson*, 1992; *Ebinger et al.*, 1997; *Foster et al.*, 1997]. The Western Rift is characterized by several ~100-km-long en echelon fault-bounded basins [*Ebinger et al.*, 1989]. Most of the Cenozoic rift system to the south and southwest of the Tanzania craton developed within or adjacent to the Karoo rift system.

1.1.1. Crust and Mantle Structure

[7] Until recently, investigations of crustal structure in East Africa focused primarily on the Eastern and Western Rifts. Early studies used seismic refraction data and observations from teleseismic and regional earthquakes to examine crust and mantle structure. These studies yielded 40–48 km Moho depth estimates beneath unrifted crust and 20- to 32-km depths under the rift valleys (see review by *Nyblade* [2002] and references therein). We discuss more recent results below.

1.1.2. Kenya

[8] Crust and mantle structure beneath and adjacent to the Kenya Rift was investigated by the Kenya Rift International Seismic Project (KRISP) using seismic refraction profiles [*Prodehl et al.*, 1994; *Fuchs et al.*, 1997]. The KRISP group found that along the axis of the rift, the Moho depth shallows from 35 km in southern Kenya to ~20 km beneath northern Kenya. Away from the rift, the crust thickens to ~37 km beneath the Tanzania craton, and ~38 km beneath the Mozambique Belt. Teleseismic receiver functions and Rayleigh wave dispersion measurements [*Last et al.*, 1997] give similar Moho depths of ~40 km and ~38 km for the Tanzania craton and Mozambique Belt.

[9] The KRISP group found low *Pn* velocities of ~7.7 km/s under the axis of the rift, and *Pn* velocities of ~8.2 km/s under the Tanzania craton and Mozambique Belt. The transition from low to high *Pn* velocities is abrupt, and coincides with the main rift border faults, suggesting that tectonic and/or magmatic modification of uppermost mantle structure is confined in Kenya to the rift proper.

[10] Inversions of teleseismic travel time residuals for lithospheric structure beneath the Kenya Rift suggest that the mantle lithosphere there has been removed or highly modified [*Green et al.*, 1991; *Achauer et al.*, 1994; *Slack et al.*, 1994]. There are two interpretations for the structure away from the rift. *Green et al.* [1991] and *Achauer et al.* [1994] found evidence for a steep-sided low-velocity channel beneath the rift from ~80 km to at least 200 km depth, implying that lithospheric thinning has been mostly accommodated via rift extension. However, *Slack et al.* [1994] found evidence for a much broader upwelling of the asthenosphere/lithosphere boundary such that much of the lithospheric mantle away from the rift has been modified.

1.1.3. Tanzania

[11] Crust and mantle structure beneath the craton and rifted orogenic belts in Tanzania has been investigated in a number of studies using data from the Tanzania Broadband Seismic Experiment [*Nyblade et al.*, 1996]. *P* wave travel times from regional earthquakes were inverted for long-wavelength (>100 km) *Pn* velocity variations beneath Tanzania by *Brazier et al.* [2000]. They found *Pn* velocities of ~8.4 km/s beneath the center of the Tanzania craton, 8.3 km/s beneath the Mozambique Belt where the Eastern Rift terminates, and 8.4 km/s beneath the Western Rift.

[12] Structure deeper in the upper mantle beneath the orogenic belts and craton in Tanzania has been modeled by inverting relative travel times of teleseismic *P* and *S* waves [*Ritsema et al.*, 1998] and Rayleigh wave phase velocities [*Weeraratne et al.*, 2003] for upper mantle seismic velocity variations and by geographically stacking receiver functions to image topography on the 410- and 660-km discontinuities [*Owens et al.*, 2000]. A low-velocity zone is found under the craton at ~170 km depth. Beneath the adjacent rifted mobile belts a low-velocity zone begins at ~80 km and extends to at least 300 km depth.

[13] *Last et al.* [1997] analyzed receiver functions and Rayleigh waves and found a Moho depth of ~43 km beneath the Ubendian Belt. *Nolet and Mueller* [1982] examined mantle structure beneath the Western Rift by simultaneously inverting teleseismic body wave travel times and surface wave phase and group velocities and found a thin ~20-km lithospheric mantle underlain by a low-velocity channel, suggesting extreme local lithospheric thinning.

1.2. Deformation, Anisotropy, and Teleseismic Shear Wave Splitting

[14] Olivine is a seismically anisotropic mineral that comprises a significant fraction of the upper mantle. It has a maximum *P* and *S* wave seismic velocity anisotropy of 25% and 12%, respectively [*Kumazawa and Anderson*, 1969]. When an aggregate of olivine grains is deformed via dislocation creep, a fabric or lattice preferred orientation (LPO) develops where one or more of the three olivine crystallographic axes have a preferred orientation, leading to a bulk anisotropy for the aggregate. The orientation of the bulk anisotropy depends on which set of dislocation slip planes are active in accommodating the deformation and what type of deformation is occurring [*Nicolas and Poirier*, 1976; *McKenzie*, 1979; *Nicolas and Christensen*, 1987; *Karato*, 1989; *Ribe and Yu*, 1991; *Ribe*, 1992]. For progressive simple shear the fast [100] *a* axes of olivine rotate toward the direction of shear. For uniaxial strain the fast *a*

axes rotate away from the direction of shortening and toward the direction of elongation. Therefore the fast direction of the bulk anisotropy can be a proxy for mantle flow. A bulk anisotropy can also develop because of a preferred orientation of structures such as cracks [*Crampin*, 1991] and magma-filled lenses [*Kendall*, 1994] or parallel layers of alternating seismic velocities [*Backus*, 1962].

[15] A teleseismic shear phase (plane wave) propagates through an anisotropic mantle as a pair of orthogonally polarized phases that travel at different speeds [e.g., *Christensen*, 1966]. The orientations of the polarization directions depend on the orientation of anisotropy with respect to the wave front propagation direction. The delay time (*dt*) that accumulates between the two phases is proportional to the ray path length and the magnitude of anisotropy sensed along the ray path. For a single horizontal anisotropic layer with a horizontal LPO of fast olivine *a* axes the observed fast polarization direction of a vertically traveling shear phase is horizontal and parallel to the LPO, and *dt* is proportional to the layer thickness and magnitude of anisotropy. In the case of a dipping axis of anisotropy the fast polarization direction is not in the horizontal plane [e.g., *Hartog and Schwartz*, 2000]. Because we only analyze horizontal seismograms for shear wave splitting, we only resolve the horizontal projection of the fast polarization direction, which we refer to as the fast polarization azimuth (ϕ). In the case of multiple anisotropic layers [e.g., *Silver and Savage*, 1994] the observed splitting does not correlate directly with the individual splitting that occurs in each layer. We therefore refer to the observed splitting measurements (ϕ and *dt*) as "apparent" splitting measurements. For a layer with a dipping fast axis or two sublayers of different anisotropy the apparent splitting measurements will change in a predictable fashion as a function of initial polarization azimuth, back azimuth, and incidence angle. Therefore apparent splitting measurements can yield important insights into the kinematics and magnitude of active and past deformation in the Earth's interior.

1.3. Previous Shear Wave Splitting Results

[16] Shear wave splitting measurements previously reported for East Africa come from Kenya [*Gao et al.*, 1997; *Barruol and Ismail*, 2001]. *Gao et al.* [1997] analyzed up to four events per station on 17 short-period seismic stations of the 1989/1990 KRISP project (Figure 1). The stations were located within and on the flanks of the Kenya Rift, above the Kenya dome. A total of eight events were analyzed, and all came from a back azimuth window between 060° and 090°, with ϕ subparallel to the strike of the Kenya Rift and *dt* between 0.8 and 2.4 s (average is 023° ± 16°/1.5 ± 0.5 s). Gao et al. favored an interpretation wherein ϕ resulted from vertical magma-filled lenses in the lithosphere striking in the direction perpendicular to the extension direction.

[17] In the same region, *Barruol and Ismail* [2001] measured *SKS* splitting and calculated single-layer anisotropy models with a horizontal fast axis for Global Seismic Network (GSN) broadband stations KMBO and NAI (Figure 1). They analyzed 64 events for KMBO, and five events for NAI. They found consistent models at both stations (340° ± 8°/1.0 ± 0.3 s). However, they showed that there was a large scatter in the apparent splitting measurements at KMBO, suggesting that the single-layer model was only an approximation of a more complicated anisotropy at depth. They favored an interpretation of a combination of magma-filled lenses and LPO due to rift-parallel mantle flow, complicated by three-dimensional heterogeneity, dipping structures, and/or lithospheric anisotropy. Even though these two studies are seemingly inconsistent, we will show later that this difference between KRISP and NAI/KMBO is part of a spatially consistent pattern where stations demonstrate moderate splitting perturbations from that due to an average mantle fabric with a N/S fast direction.

1.4. New Broadband Seismic Data

[18] We analyze and model shear wave splitting of teleseismic waveforms recorded by broadband seismic stations in Tanzania and Kenya (Figure 1). Data for this study come from the Tanzania Broadband Seismic Experiment [*Nyblade et al.*, 1996] and the Kenya Broadband Seismic Experiment [*Nyblade and Langston*, 2002]. In the Tanzania experiment, 20 seismic instruments were deployed for 1 year (1994–1995) along two transects crossing the East African Plateau and bordering orogenic belts from east to west and northeast to southwest. In the Kenya experiment, 10 broadband seismic stations were located in orogenic belts and operated for 1 year between July 2001 and July 2002. In addition, we also analyze and model splitting at GSN stations KMBO, MBAR, and NAI. KMBO and NAI are on volcanic fields associated with the Kenya Rift, and MBAR is located in the Paleoproterozoic Ruwenzori Belt in Uganda.

[19] We analyze 205 unique events (Table 1 of auxiliary material[1]) recorded on at least one of the stations, for a total of 888 phases: *SKS* (69%), *SKKS* (12%), *PKS* (13%), and direct *S* (6%) (Table 2 of auxiliary material).[1] The events recorded on MBAR and the Tanzania stations have a good to fair distribution of back azimuths (BAZ) (Figure 2). The initial polarization azimuth (IPA) has a modulo 180° ambiguity. Because we mostly analyze core-refracted phases, which obtain IPAs that are parallel to BAZs, the events have a very good distribution of IPA. The events recorded on NAI, KMBO, and the Kenya stations have a poor-to-fair distribution of BAZ and a good distribution of IPA. (Owing to an unknown problem with assembling the KMBO data set we were only able to analyze 29 events recorded on that station between 1995 and 2002, although more data do exist [e.g., *Barruol and Ismail*, 2001].) All analyzed phases have steeply dipping incidence angles (INC) of 5°–27° and sample the upper mantle almost directly beneath the station, providing very good lateral resolution. The coverage in BAZ, IPA, and INC is not ideal but is probably sufficient to discriminate between splitting from a single-layer model with a horizontal or dipping fast axis and a two-layer model with horizontal fast axes. The INC range is probably only sufficient to resolve single layers of anisotropy with dipping fast axes for most dips.

2. Methodology: Apparent Splitting Measurements

[20] The delay time (*dt*) between fast and slow split waves is $dt = \frac{dv}{v}L$, where *dv* is the strength of anisotropy

[1] Auxiliary material is available at ftp://ftp.agu.org/apend/jb/2003JB002866.

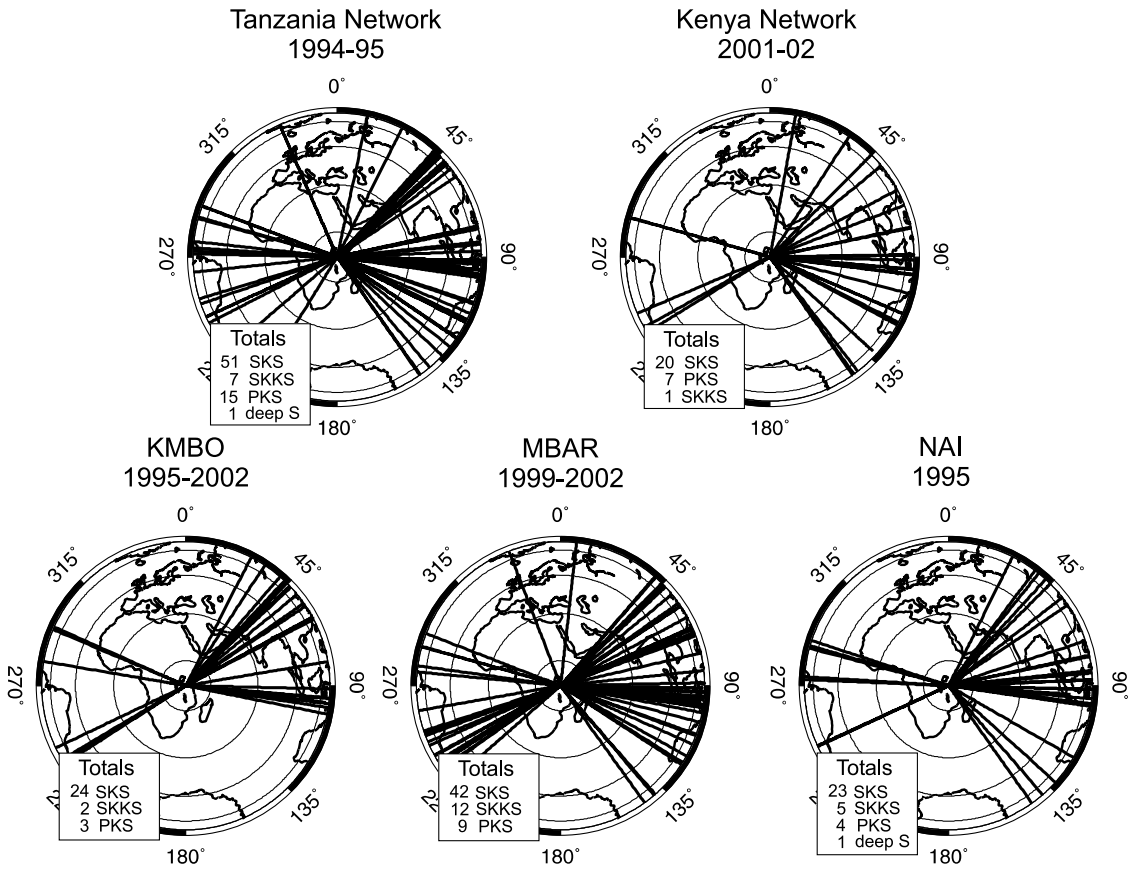

Figure 2. Map showing great circle paths from epicenters to the stations in East Africa for earthquakes analyzed for shear wave splitting and recorded on the Tanzania Network, Kenya Network, and GSN stations KMBO, MBAR, and NAI. We analyzed a subset of these events at each station because of station-varying signal-to-noise ratios (17–59 events for Tanzania and 2–15 events for Kenya). For some events, two phases were analyzed (e.g., *PKS* and *SKKS*); the predominant phase is indicated in the totals. See Table 1 of auxiliary material.

(difference between the two *S* wave velocities), *v* is the mean shear wave velocity (~4.5 km/s between 0- and 300-km depth), and *L* is the layer thickness. Because *dt* is an integrated measure of anisotropy along the ray path, it cannot be used to uniquely constrain the location of anisotropy. However, we can make inferences about the location of anisotropy. The core-refracted phases travel through the outer core as compressional phases and acquire their initial shear polarization direction during a *P*-to-*S* conversion at the core-mantle boundary (CMB) when they exit the core. Splitting of core-refracted phases must therefore be derived from anisotropy along the ray path from the CMB piercing point to the seismic station. The direct *S* phases obtain their initial polarization at the source. We are only interested in anisotropy beneath the seismic station, and we therefore reduce the possibility of source-side splitting by analyzing direct *S* events only from hypocenters deeper than 550 km, a depth beneath the possible effects of significant upper transition zone anisotropy found in some subduction zones [*Fouch and Fischer*, 1996]. We also do not analyze direct *S* phases from the Tonga-Kermadec and New Hebrides subduction zones, as evidence of strong source-side splitting has been reported for that region [*Wookey et al.*, 2002]. Because the strongest azimuthal anisotropy observed by surface waves occurs between 50 and 300 km in most places [*Montagner*, 1994; *Montagner and Guillot*, 2000], one can generally constrain the location of the majority of anisotropy to this depth range.

[21] We use a modified version of the method of *Silver and Chan* [1991] to make apparent splitting measurements of phases with an energy signal-to-noise ratio (SNR) >15. For simplicity, we refer to the horizontal components parallel and perpendicular to IPA as the ''radial'' and ''transverse'' components, respectively, although this is strictly only true for the core-refracted phases. We define SNR as the ratio of the observed radial energy to the observed transverse noise energy, which is equivalent to the square of the amplitude SNR. We used the first 100 s prior to the picked time window to calculate the noise energy and normalized both energy calculations by their respective window lengths. We assume that the effects of scattering due to mantle discontinuities are negligible, which is probably a reasonable assumption in this study given the general lack of distinct, coherent energy that follows the analyzed phases.

[22] Figures 3a and 3b show the results of splitting analyses for examples of high and low SNR for constrained measurements (the 95% confidence region is closed). For each event we band-pass filter the waveforms between 0.02 and 0.2 Hz and pick a master time window around the

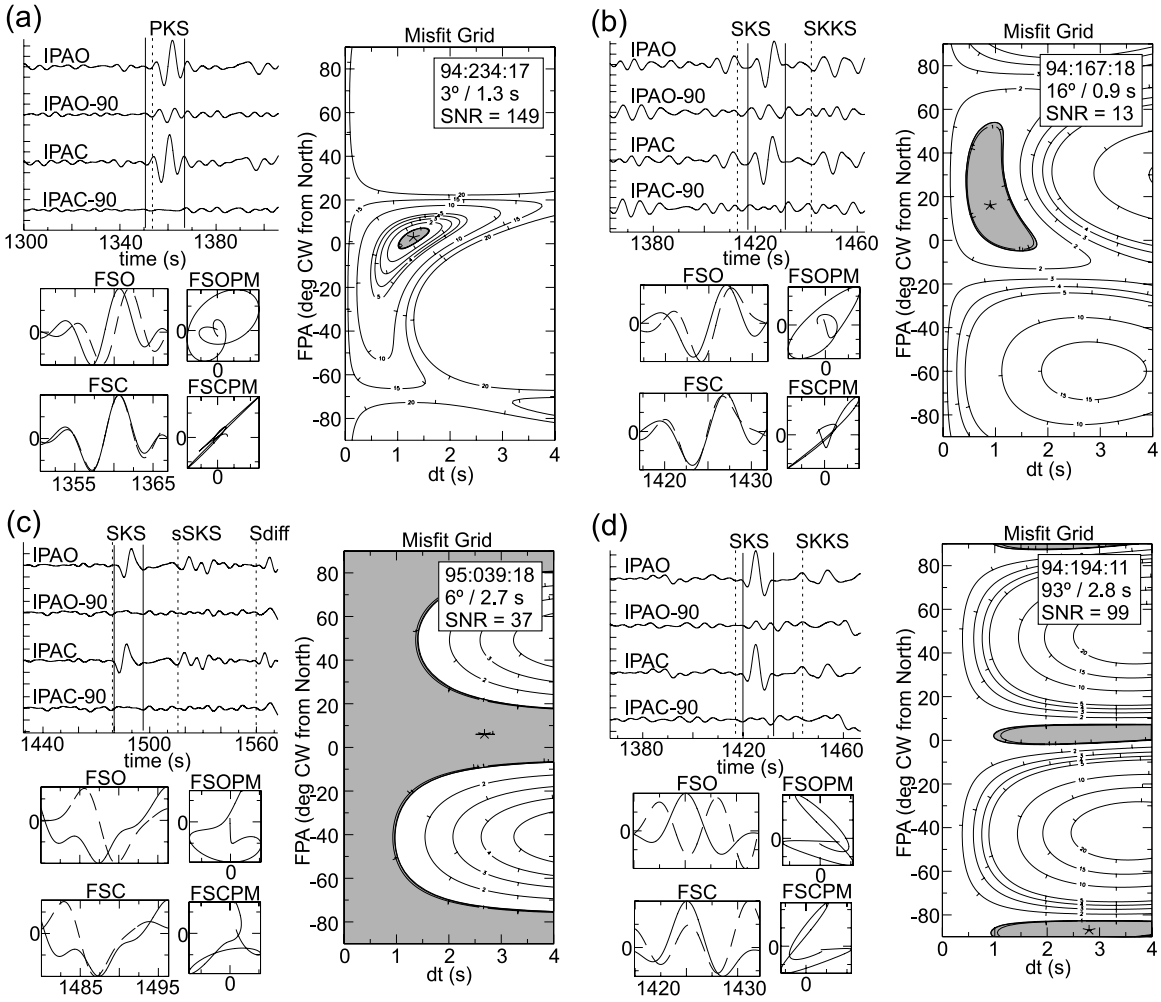

Figure 3. Four examples of apparent splitting analyses for station GOMA along the western branch of the East African rift system in Tanzania. For each example we show the initial polarization azimuth and orthogonal complement of the original waveforms (IPAO and IPAO-90) and the anisotropy-corrected waveforms (IPAC and IPAC-90). Dashed lines indicate the IASP91 predicted phase arrival times. Vertical solid lines indicate the picked time window. If the apparent splitting parameters predict perfectly the observed splitting, no energy should remain within the time window of the IPAC-90 component. Beneath these four traces are the fast/slow waves and corresponding particle motions for the original (FSO and FSOPM) and anisotropy-corrected waveforms (FSC and FSCPM). The misfit grid shows the minimum or minima found in this search for the optimum fast polarization azimuths (FPA) and delay time (*dt*) that minimizes the energy on the IPAC-90 component. The text in the upper right of the misfit grid indicates the event analyzed (year:julian day:hour), the optimum apparent splitting parameters, and the radial-signal-to-transverse-noise energy ratio (SNR). We show constrained splitting examples of phases with (a) high SNR and (b) low SNR (we only measure phases with energy SNR > 15), and unconstrained splitting measurements (ucons) due to (c) no significant apparent splitting and/or (d) unclosed and repetitive confidence regions.

phase. Then we create 30 different time windows by randomly perturbing the master time window boundaries by up to ±20% of the length of the master time window. For each of these 30 windows we either (1) assume the initial polarization azimuth (IPA) is equal to the back azimuth (BAZ) and search over trial apparent fast azimuth (ϕ) and delay time (*dt*) for the optimum parameters that best remove the energy from the anisotropy-corrected transverse component of the core-refracted phases or (2) calculate the IPA directly from the data and search for the optimum parameters that maximize the similarity between trial fast/slow waves for the direct *S* phases [*Silver and Chan*, 1991]. For each of the 30 analyses the number of degrees of freedom *N* is calculated directly from the windowed data [*Silver and Chan*, 1991]. Then we stack the 30 misfit grids *M*, find the global minimum, and derive the 95% confidence region from the average number of degrees of freedom ($\overline{N}$) using $\frac{M_s(m)}{M_s(m_{\text{opt}})} \leq 1 + \frac{k}{\overline{N}-k} f_{k,\overline{N}}(1-\alpha)$, where M_s is the stacked misfit grid, m is the model, m_{opt} is the optimum model, $k = 2$ is the number of model parameters, f is the inverse of the F distribution, and $\alpha = 0.05$

[*Jenkins and Watts*, 1969]. This is the same procedure used by *Wolfe and Silver* [1998] to calculate a constrained station splitting estimate from stacking misfit grids from different events. Apparent splitting measurements and confidence regions estimated from standard techniques are sometimes significantly affected by small perturbations in the picked time window. Through simple averaging this grid-stacking modification increases the stability of the apparent-splitting-analysis method and attenuates the effect of the perturbations.

3. Apparent Splitting Results

[23] In this section, we describe the splitting complexity at each station as a function of back azimuth, initial polarization azimuth, and incidence angle. We then inverse model the stations for which complexity is observed and use statistics and qualitative reasoning to determine which model, if any, is the best. We then briefly summarize our modeling results and show that the complexity is best interpreted as due to minor lateral and vertical variation of a single-layer anisotropy model with a horizontal fast axis.

[24] About 60% of the phases we analyzed did not demonstrate detectable apparent splitting and yielded unconstrained measurements (e.g., Figures 3c and 3d). Lack of apparent splitting can occur for a variety of reasons: (1) The Earth beneath the station is isotropic to steeply incident shear phases; (2) simple anisotropy exists, and the IPA is parallel or perpendicular to the fast axis; (3) complex anisotropy exists, and interference between multiply split phases creates a complicated waveform that is not explained well by the optimum apparent splitting parameters, (4) the signal does not contain an adequate frequency bandwidth to calculate the error bars, perhaps because of large earthquake source dimensions, attenuation along the ray path, and/or intracrustal scattering/reverberation; or (5) the SNR is too low. For cases 2 and 3 these measurements are traditionally referred to as "nulls." Eliminating the fifth possibility by keeping only those events with SNR > 15, we keep all unconstrained measurements and refer to them as "ucons" for convenience. However, there are other methods to help distinguish between ucons and nulls (e.g., D. Schutt, personal communication, 2003).

[25] To investigate the complexity in the splitting measurements, we show rose diagrams of the constrained ϕ for each station in Figure 4. We observe inconsistent splitting at stations INZA and MBAR in the west; PUGE, MBWE, SING, MTOR, and RUNG on the craton; KOND, KOMO, and KIBE in the east; MTAN, PAND, and TUND in the south; and KMBO and KITU in the north. The majority of the stations with complex splitting are found on the craton. The most consistent splitting occurs for Kenya stations, with ϕ oriented between NNW/SSE and NE/SW. Although most Kenya stations did not record as many events as the other stations and therefore our conclusion that splitting in Kenya is more consistent than in Tanzania may be premature, splitting is fairly to very consistent at nearby GSN station NAI, which recorded many more events.

3.1. Variations as a Function of Back Azimuth

[26] To investigate in more detail the complexity in splitting that is clearly present at several stations, we show the apparent splitting measurements as a function of BAZ and INC (Figure 5). This variation could result from a single layer of anisotropy with a dipping fast axis [*Chevrot and van der Hilst*, 2003], spatially variable anisotropy within the station Fresnel zone [*Alsina and Snieder*, 1995; *Rümpker and Ryberg*, 2000], or more complicated anisotropy [*Babuška et al.*, 1993; *Saltzer et al.*, 2000]. This visualization reveals trends in ϕ at several stations (bold) where strong complexity was identified in Figure 4 (shaded circles). From west to east BAZ, ϕ for stations KOND, MTOR, and SING (east side of craton) rotate from ~WNW–NW for arrivals from the west, through the craton, to N–NNE for arrivals from the east beneath the rift or mobile belts. For INZA and PAND (west and south side of craton), ϕ show a comparable, almost mirror-image rotation from N–NE to E–ESE. Station MBAR in Uganda shows N–NE ϕ for southwest BAZ but a NE-to-NNW ϕ rotation for southeast to northeast BAZ.

[27] The number of ucons as a proportion of all measurements recorded at each Tanzania station varies, apparently randomly, between 35% (URAM) and 91% (KIBE), with the highest percentage observed at KIBE (91%), MBWE (83%), RUNG (77%), and MTAN (76%). Splitting beneath the Kenya stations is more consistent, and the number of ucons (not including ANGA for which only two events were analyzed) varies between 25% (KIBO) and 60% (TALE). For most stations the ucons do not originate from a consistent BAZ or INC. In fact, ucons appear to come from random BAZ and INC and sometimes occur for ray paths that were similar to other ray paths that resulted in constrained splitting measurements (e.g., MTOR). This suggests that the ucons may be associated with splitting of signals of low-frequency bandwidth, or other effects such as crustal scattering may be complicating the splitting signal. However, the ucons could also be an indication of anisotropic complexity. Constrained inconsistent splitting is clearly observed at some of these stations, which is evidence for anisotropic complexity, either vertically and/or laterally. However, anisotropic complexity alone cannot easily explain two core-refracted phases (both with good SNR) with the same BAZ and INC that yield respectively a constrained measurement and ucon.

[28] We inverse model splitting at each station for a single layer of anisotropy with a dipping fast axis to attempt to explain coherent ϕ variations with BAZ and INC (Figure 5). A grid search is performed at each station for the three optimum angles that best orient (with respect to the ray paths associated with the analyzed phases) an olivine and mafic kimberlite nodule tensor [*Mainprice and Silver*, 1993] to explain the observed splitting. We compare the fit of models by calculating the variance reduction (R) and Akaike's Information Criterion (AIC) [*Burnham and Anderson*, 2002] for all models. In summary, both optimum model layer thicknesses at each station are quite different, with averages of ~170 km for the olivine model and ~780 km for the nodule model, and between adjacent stations the thicknesses for one model type vary greatly. Although both models predict a considerable amount of the observed variation, we do not think these models are realistic. The

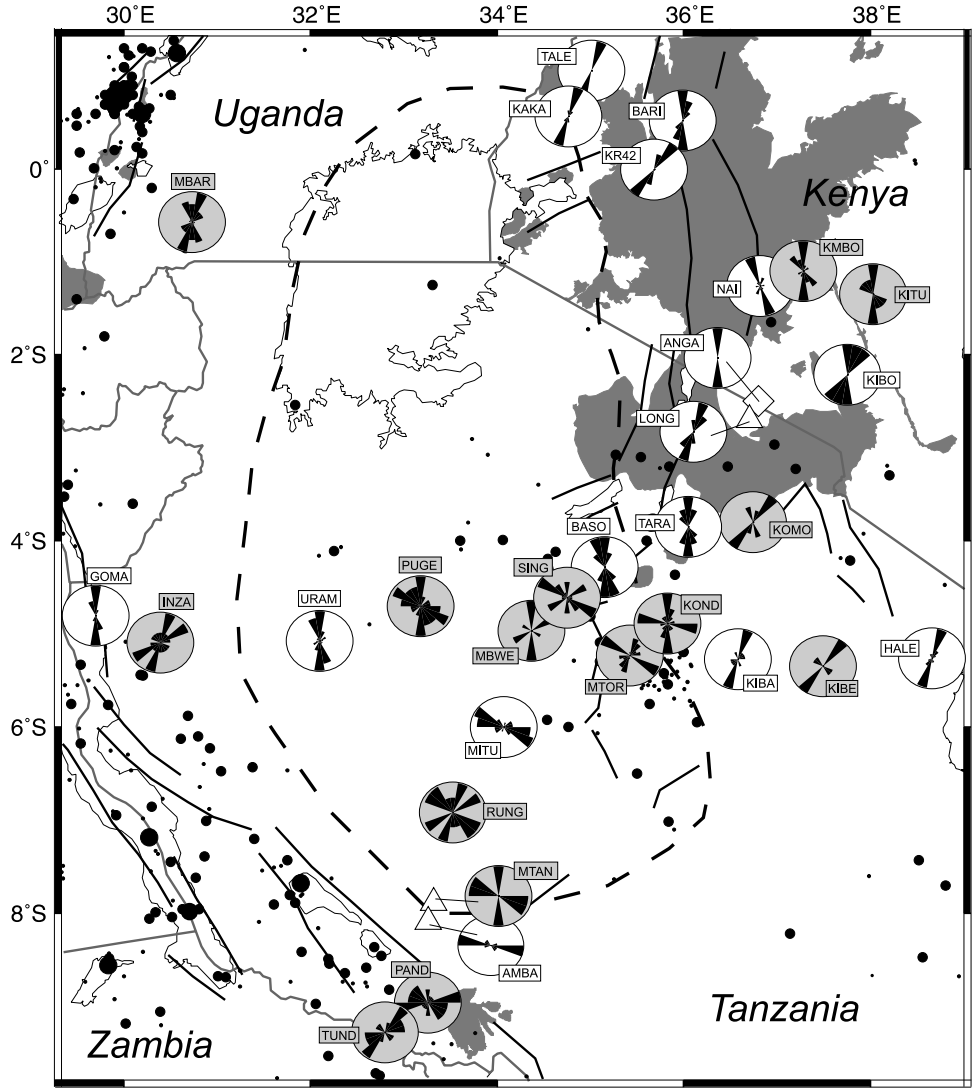

Figure 4. Rose diagrams of constrained splitting fast azimuths. The 360° circle was divided into 20° sectors. The length of each sector is proportional to the number of fast polarization azimuths that were contained in that sector. Error bars associated with each measurement are ignored. The ucons are not included because of the ambiguity associated with their meaning. For stations that recorded consistent ϕ, the rose diagram contains one dominant sector pointing toward ϕ (and its 180° equivalent). Multiple sectors indicate inconsistent splitting (shaded circles). The geology and seismicity symbols are the same as in Figure 1.

variations that we see could be explained by laterally and possibly vertically varying, horizontal fast axis anisotropy beneath each station, but the magnitude of such variation is difficult to estimate.

3.2. Variations as a Function of Initial Polarization Azimuth

[29] *Silver and Savage* [1994] showed that for vertically incident shear waves, two vertically stacked horizontal layers of anisotropy with horizontal fast directions lead to a predictable variation with a 90° periodicity in apparent splitting measurements as a function of IPA. *Rümpker and Silver* [1998] showed that such variations also occur for relatively long-period signals ($T/dt \geq 5$) passing through a medium with a smooth, vertically varying anisotropy from one fast direction at the bottom to another at the top. The dominant period of our teleseismic signals is ~10 s, and therefore our data fit this criterion for *dt* up to 2.0 s. Therefore, if a simple two-layer or smoothly varying anisotropy exists, we should be able to detect it.

[30] Figure 6 shows plots of the apparent splitting measurements versus IPA for all stations. It is important to note that the *y* axis (ϕ) wraps around 180°. Most stations show no obvious pattern. However, stations MITU, MTOR, PUGE, and SING (bold) demonstrate trends in ϕ and/or *dt*. The 90° periodicity zones expected for two-layer models are not obvious in these trends, but the event IPA distributions for stations PUGE and SING do not permit the resolution of such a trend if one exists.

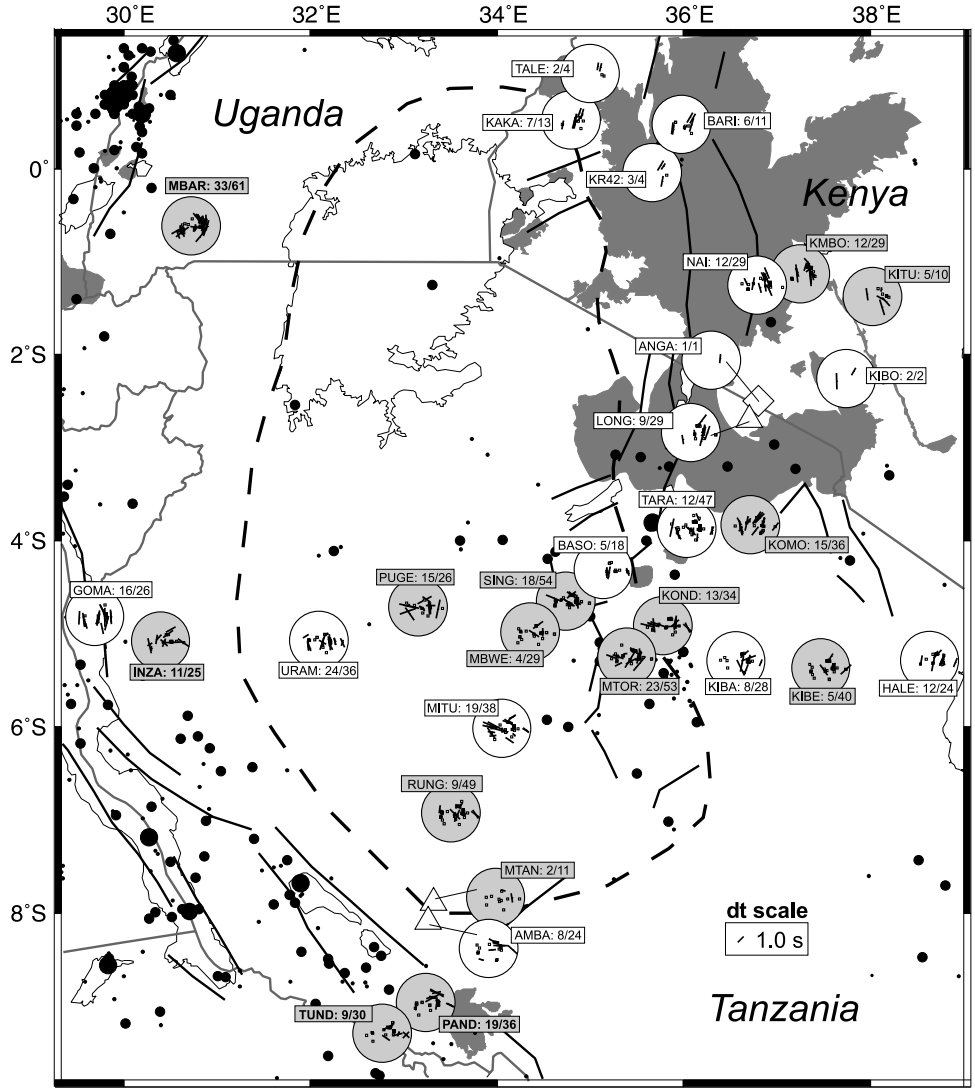

Figure 5. Polar plots showing variations in apparent splitting with back azimuth (angle) and incidence angle (radius, maximum = 30°). Lines represent constrained splitting measurement, their orientation parallel to the fast polarization azimuth and length proportional to the delay time (see scale). Ucons are shown as small squares inside the polar plots. The fraction next to the station name indicates the number of constrained measurements (numerator) out of the total number of analyzed phases (denominator). The difference between the numerator and denominator indicates the number of ucons. Bold stations demonstrate a possible trend (see text). Shaded circles are the same as in Figure 4.

[31] Assuming that the anisotropy beneath each station is uniform within the Fresnel zone at all depths and that the difference between our subvertical rays (INC = 5°–27°) and the vertical is negligible, we use the apparent-splitting-measurement analytical expressions derived by *Silver and Savage* [1994] and perform a grid search over the four trial parameters (ϕ and dt for both upper and lower layers) to determine the optimum two-layer anisotropy model with horizontal fast axes for a dominant signal frequency of 0.1 Hz. The thicknesses of these layers cannot be uniquely determined, but dt is proportional to the layer thickness and percent anisotropy. We used two different data sets in this modeling: constrained measurements with ucons (YUCONS) and constrained measurements without ucons (NUCONS).

[32] The two-layer modeling results for both data sets are presented in Table 3 of the auxiliary material. The best models (those with $R \geq 0.50$) are also plotted in Figure 6 (INZA, KIBA, KIBE, KOND, MBWE, PAND, KR42, and KMBO). The strongest evidence for a two-layer model comes from stations KOND (R = 0.89) and KMBO (R = 0.75). Although a considerable amount of this for KMBO is due to one ϕ measurement at an IPA = 60°, it is interesting that a similar model is also predicted for nearby station KR42 (Table 3 in auxiliary material). The AIC values suggest the TL models predict the data better for stations MITU and PUGE. However, the R values for these models are too small for us to consider significant ($R \leq 0.36$). Thus taking into account both AIC and R, TL models do not predict the data at stations MITU, MTOR, PUGE, and

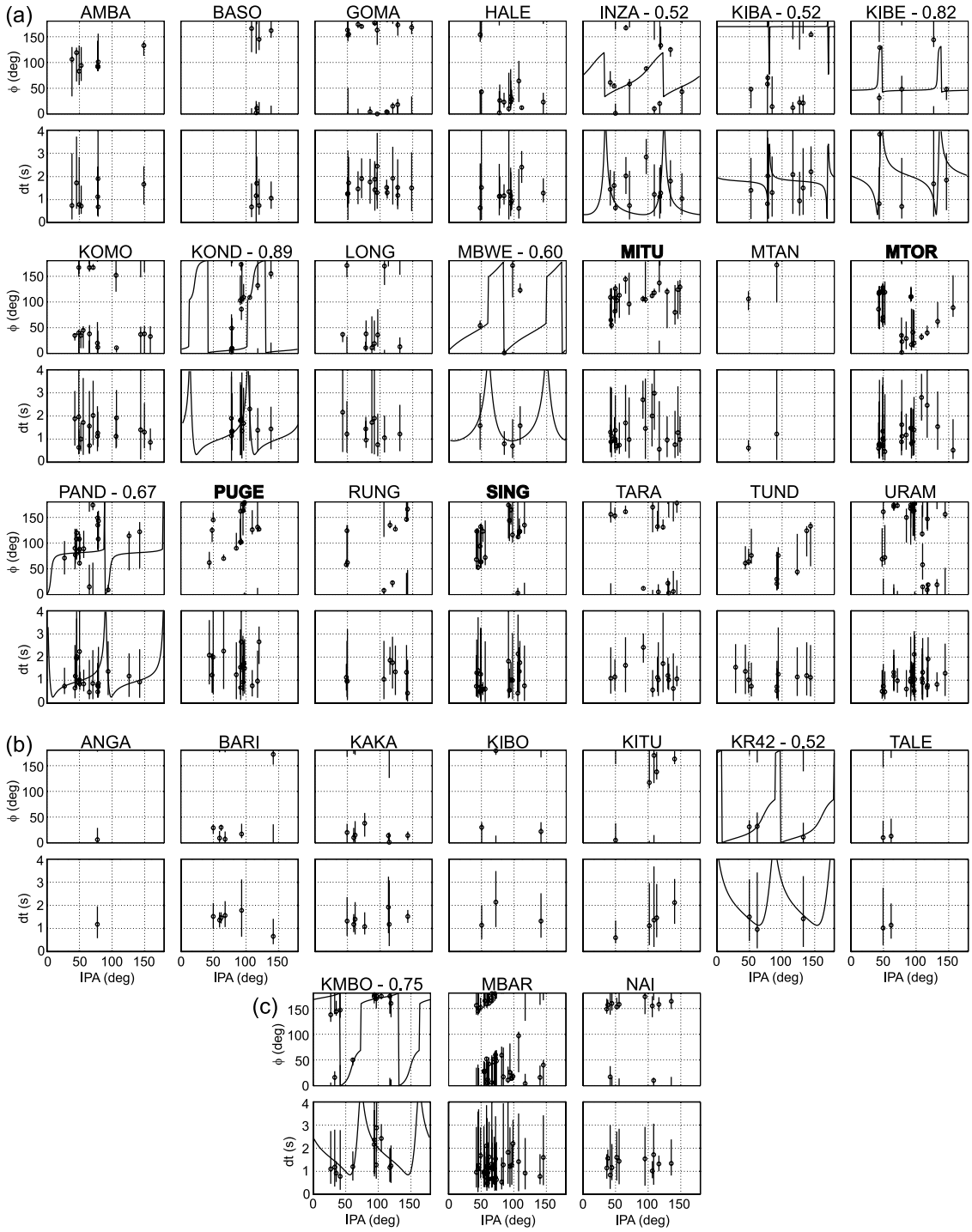

Figure 6. Variations in apparent splitting parameters (circles with 2σ error bars) as a function of initial polarization azimuth for the (a) Tanzania Network, (b) Kenya Network, and (c) GSN stations. Bold stations demonstrate a visible trend. The optimum two-layer models are shown for stations with $R > 0.50$.

SING significantly better than that provided by the optimum single-layer model with a horizontal fast axis.

3.3. Model Comparison

[33] In summary, the degree to which splitting complexity is predicted by dipping-axis (DA) and two-layer (TL) models, two model types that lead to very different interpretations, varies considerably between stations (Figures 7a and 7b and Table 3 in auxiliary material). For many stations both models explain the data equally well. The fact that grid searches for the optimum TL and DA models produce a few possible solutions and many more local minima suggest that the current data sets do not permit an inversion for a unique TL or DA model. Similarly for the dipping-axis and two-layer models (except in Kenya), between adjacent stations for each model type, there is no convincing consistency that

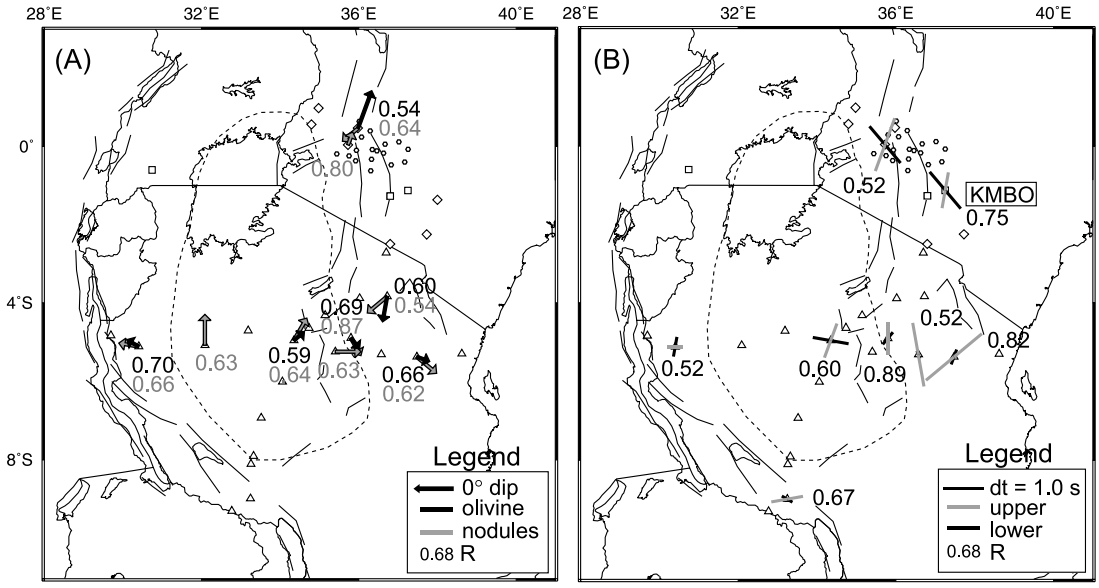

Figure 7. Comparison of more complicated anisotropy models. We show the best model for stations that have at least one model that fits the data with $R > 0.50$. (a) Single-layer models with a dipping fast axis. The direction and length of the arrow indicates the azimuth and dip of the fast axis in a lower hemisphere projection. Solid indicates orthorhombic olivine, and shaded indicates an average mafic kimberlite-nodule tensor [*Mainprice and Silver*, 1993], which has an approximately monoclinic symmetry for fast polarization azimuths and a much smaller anisotropy than pure olivine. (B) Two-layer modeling using two different data sets (constrained measurements without ucons (NUCONS) and with ucons (YUCONS)). For each station the better of these models is shown. These lines are parallel to the model fast direction, and their length is proportional to model delay time. Shaded and solid indicate upper and lower layer splitting, respectively.

one might expect given that most tectonic and magmatic processes in the region probably occurred over scales that are larger than the spacing of the stations. Only plotting the best model (of the DA and TL models) for each station would show an even greater spatial inconsistency. Collectively, our observations and modeling results suggest that DA and TL models are inappropriate models for this region and that there are lateral and possibly vertical variations in anisotropy.

3.4. Stacked Station Splitting Estimates (Horizontal-Axis Modeling)

[34] Because we find evidence for lateral variations in anisotropy, we assume that the variation is minor and prefer to approximate the anisotropy beneath each station as due to a horizontal axis (HA) model using the stacking method of *Wolfe and Silver* [1998]. This model therefore gives us the first-order approximation to the true, more complicated solution by averaging out the effects of minor lateral anisotropy variations, a conclusion supported by the waveform modeling results of *Rümpker and Ryberg* [2000]. Such a first-order approximation should also provide us with a means to smooth out the effects of crustal scattering, which would be strongly dependent on BAZ and INC.

[35] The *Wolfe and Silver* [1998] stacking method was developed to derive HA models for stations plagued by high levels of seismic noise and for which few good events have been recorded. The technique works by summing the misfit grids for each splitting measurement at a particular station and using the total number of degrees of freedom to calculate the new critical 2σ threshold that uniquely defines the 95% confidence region surrounding the global minimum (the optimum HA model). The uncertainty is normally assumed to be due to data error. However, the technique can also be used in situations where the uncertainty is assumed to be due to model error, i.e., for stations with low levels of seismic noise but significant apparent splitting measurements variations. Because of the low noise levels for these cases and because of the observations of similar ray paths yielding both ucons and constrained splitting measurements, we feel the ucons should receive less weight.

[36] We again divide the apparent splitting measurements into two subgroups: with ucons (YUCONS) and without ucons (NUCONS). The stacking results for both subgroups of data are presented in Table 3 in the auxiliary material, and results for the NUCONS data set are shown in Figures 8 and 9. Figures 8 and 9 compare the station splitting estimates to other types of geological and geophysical data conducive to comparing different anisotropy-source hypotheses. It should be noted that these HA solutions are not identical to those used to calculate M_o in the R calculations for the DA and TL models because the latter HA solutions were derived via a different method (and the misfit has a different definition).

[37] The station fast directions (ϕ) vary smoothly within two distinct regions: on the craton and off the craton. The ϕ for on-craton stations are subparallel to the strike of geological fabrics at the surface (Figure 8) and absolute plate motion (Figure 9). The ϕ for off-craton stations are subparallel to the strikes of geological fabrics, the nearby rift, and the craton boundary. To the east of the craton, ϕ varies

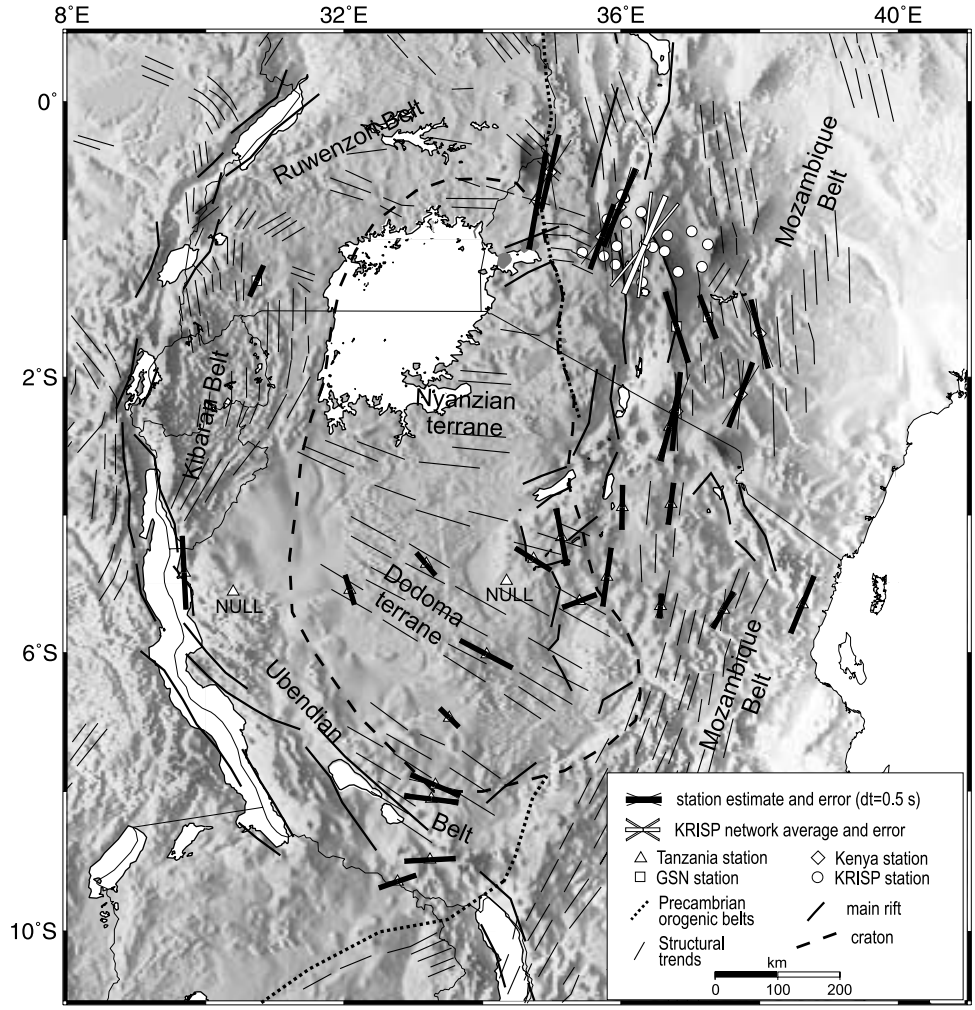

Figure 8. Single-layer station shear wave splitting models assuming horizontal fast axes (station stacked splitting estimates). The thick black lines indicate the fast direction, and their length is proportional to delay time. Overlaid upon the estimates are the geologic structural trends (thin lines) observed at the surface [*Holmes*, 1951; *Cahen et al.*, 1984; *Shackleton*, 1986; *Lenoir et al.*, 1994]. These structural trends are associated with Precambrian orogenic belts.

between NNW and NNE and is consistent with that found in the rift by *Gao et al.* [1997] and *Barruol and Ismail* [2001]. There appears to be no consistent difference in ϕ between stations inside and outside the rift.

[38] The *dt* throughout the study region varies considerably, from 0.7–1.4 s in Kenya to 0.3–0.8 s on the craton, similar to that found for splitting on the Kaapvaal and Zimbabwe cratons in South Africa [*Silver et al.*, 2001; *Fouch et al.*, 2004]. Our *dt* in and along the flanks within 30 km of the Kenya Rift range between 1.0 and 1.2 s and are consistent with the 1.5 ± 0.5–s average observed by *Gao et al.* [1997] and with the 1.0-s estimate found at nearby KMBO and NAI by *Barruol and Ismail* [2001]. There exists a trend of decreasing *dt* from Kenya toward the south to KIBA (0.4 s) in eastern Tanzania. Another trend of increasing *dt* exists from KIBA toward the east to station HALE (0.9 s). The *dt* at station GOMA adjacent to the Western Rift is 1.0 s. Farther north at MBAR in the belt between the rift and craton, *dt* is smaller (~0.5 s).

[39] If a signficant difference in splitting exists between adjacent stations, Fresnel zone calculations can be used to quantify the minimum lateral extent of a homogeneous anisotropic region as a function of depth. In principle, this could allow one to calculate the maximum depth of the anisotropy, above which the Fresnel zones at adjacent stations do not significantly overlap. *Rümpker and Ryberg* [2000] calculate *SKS* Fresnel zone widths, for a dominant 8-s period, of ~75 km at 0-km depth, 100 km at 75-km depth, 125 km at 150-km depth, and 150 km at 300-km depth. In practice, using such a method is difficult because of the ambiguity associated with how one defines the depth beneath which significant overlap begins. Furthermore, minor vertical variations in anisotropy are a source of strong bias in this approach, since a minor variation near the top of the anisotropic layer beneath one station (but not the adjacent station) could lead to the incorrect conclusion that the majority of anisotropy is much shallower than in reality. In Tanzania most on-craton stations have ~NW ϕ. However, near the eastern edge of the craton is a transition

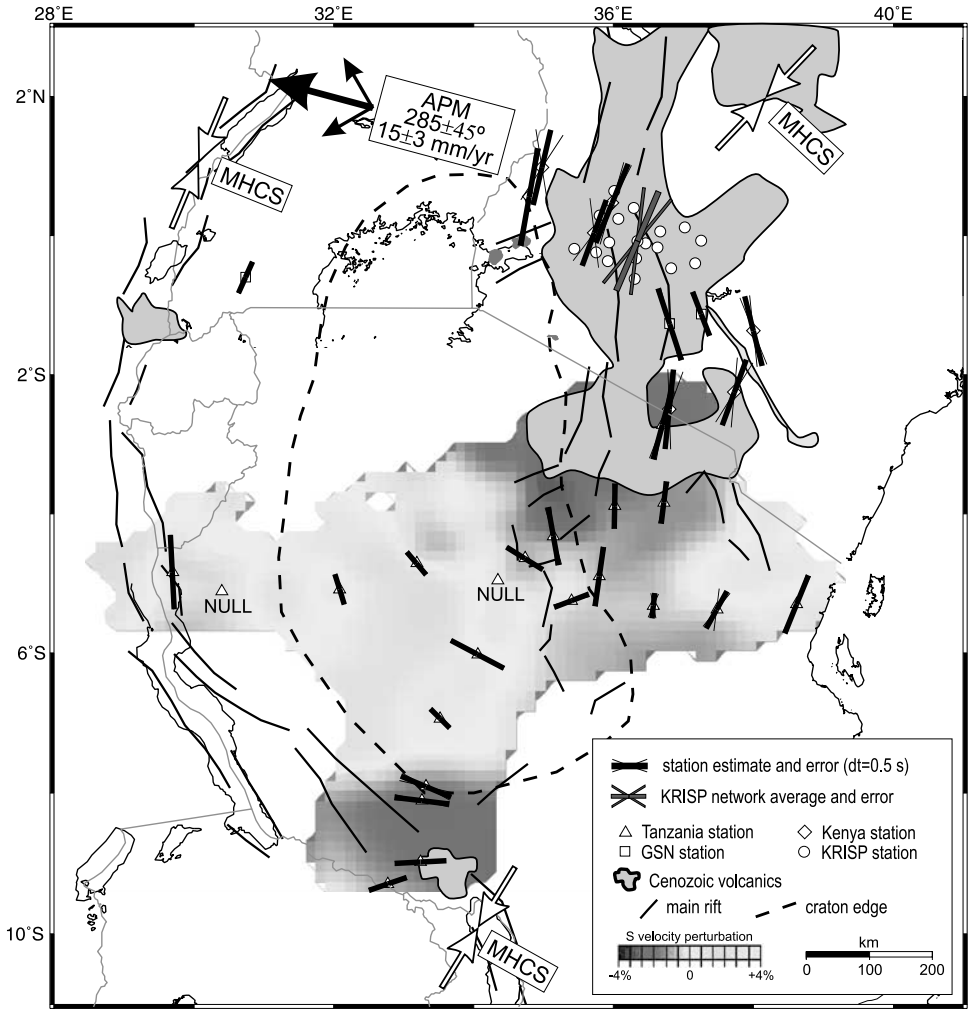

Figure 9. Single-layer horizontal-axis splitting models. Color indicates shear wave velocity tomographic slice at 200 km depth [*Ritsema et al.*, 1998]. Black arrow indicates the absolute plate motion direction [*Gripp and Gordon*, 2002]. White double arrows indicate the maximum horizontal compressive stress directions (MHCS) taken from regional averages of good-quality stress measurements (B. Mueller et al., The 2000 release of the World Stress Map 2000, available at http://www.world-stress-map.org). The thick black lines indicate the fast direction (ϕ), and their length is proportional to delay time. Thin black lines indicate the 2σ error bars for ϕ, which are too small to see for most stations. See color version of this figure at back of this issue.

where ϕ changes by 65° over 50 km between KOND and MTOR. Plots of apparent splitting measurements versus BAZ and INC suggest that this is a transition region between NW/SE ϕ from back azimuths through the craton and N/S ϕ from back azimuths beneath the rift (Figure 5). Using this 50-km distance as the maximum distance over which the lateral variation occurs, the Fresnel zone estimates suggest that if the depth of significance is where 50% of the Fresnel zone areas overlap, the anisotropy must be located above ~35-km depth. The delay times, however, are generally between 0.8 and 2.0 s, which indicates this maximum anisotropy depth estimate is inaccurate and suggests there are at least minor vertical variations in anisotropy, perhaps in the uppermost mantle.

[40] A ~0.85-s change in *dt* over 100 km between INZA and GOMA is similarly observed in Figure 8. INZA is also located above a transition between a ~N/S ϕ in the west and an ~E/W ϕ in the east (Figure 5 and Figure 1 in auxiliary material). Here the Fresnel zone maximum-anisotropy-depth estimate is ~250 km using the same depth of signficance as in the earlier example.

[41] *Barruol and Ismail* [2001] calculated station estimates for GSN stations NAI and KMBO. They analyzed 64 events for KMBO and five events for NAI. We analyzed a smaller number of events for KMBO (29) over a wider time span (1995–2003) and a larger number of events for NAI (34) during its 1995 operational period. Our fast directions both for KMBO and NAI are identical to theirs. Our KMBO $dt = 0.7 \pm 0.1$ s is somewhat smaller than theirs (1.0 ± 0.1 s), but our NAI *dt* is identical to theirs, thus providing a test of the robustness of our and their results.

[42] When we include the ucons in the stacks (YUCONS data set), the same ϕ pattern emerges. However, *dt* at many Tanzania stations decrease, especially east of the craton to

below 0.3 s in some places. Such stations with $dt < 0.3$ s are considered ucon stations, making the decreasing *dt* trend from Kenya toward the south even greater. However, we feel the most useful data that contribute to the station estimates for low noise levels are the NUCONS data. We therefore regard Figures 8 and 9 as summarizing our splitting results for Kenya and Tanzania.

4. Discussion

[43] Splitting measurements provide poor depth resolution of anisotropy. Consequently, many hypotheses have been proposed to explain teleseismic shear wave splitting in the crust and mantle in stable continental interiors, actively deforming regions, oceanic basins, and around mantle hotspots [e.g., *Crampin*, 1991; *Bormann et al.*, 1996; *Silver*, 1996; *Savage*, 1999; *Kendall*, 2000]. We examine the plausibility of the most appropriate of these hypotheses to explain our splitting data: (1) mantle anisotropy induced by extension due to a LPO of olivine, (2) anisotropy due to an alignment of parallel dikes or melt-filled lenses, (3) fossilized anisotropy in the lithospheric mantle from previous orogenic events, and (4) mantle anisotropy due to shear-related flow at the base of the lithosphere. It is important to consider all of these hypotheses because the study area is tectonically complicated and contains (1) a craton, (2) an active rift system, (3) old orogenic belts, (4) magmatism, and (5) possible proximity to at least one mantle plume. We show that most, if not all, of these contribute to the observed anisotropy in East Africa but that we can firmly rule out olivine LPO anisotropy due to ductile lithospheric stretching associated with E/W Cenozoic extension.

4.1. Mantle Anisotropy Due to Extension

[44] Ductile stretching of the mantle lithosphere should produce a lattice preferred orientation of olivine fast [100] *a* axes in the direction of extension if strain is controlled by dislocation creep [*Nicolas and Poirier*, 1976; *McKenzie*, 1979; *Christensen*, 1984; *Nicolas and Christensen*, 1987; *Ribe and Yu*, 1991; *Wenk et al.*, 1991; *Ribe*, 1992; *Mainprice and Silver*, 1993]. Such a hypothesis has been proposed to explain fast directions that are subparallel to extension directions beneath the Red Sea rift, Baikal rift, Arctic ridge, and Rhine graben [*Vinnik et al.*, 1992].

[45] Kenya and Tanzania are characterized by various styles and magnitudes of past and present extension and therefore are excellent places for studying the possible effects of extension on the development of LPO in the lithosphere. Regional averages of current maximum horizontal compressive stress (MHCS) directions from stress indicators (B. Mueller et al., The 2000 release of the World Stress Map 2000, available at http://www.world-stress-map.org) vary from NNE to NE (Figure 9). Paleostress indicators suggest a rotation from north-south to this current stress direction sometime during the Holocene [*Bosworth et al.*, 1992; *Haug and Strecker*, 1995].

[46] If the current or recent direction of lithospheric extension throughout the region is consistent with least horizontal compressive stress indicators, the fast directions should be perpendicular to the NE/SW MHCS or older Quaternary N/S compressive stress indicators. The fast directions for the on-craton stations are roughly perpendicular to these predicted directions, but because there are few signs of current or recent extensional deformation penetrating through the craton [*Nyblade and Brazier*, 2002], it is likely that the rough anticorrelation between NW fast directions and the NE MHCS direction is a mere coincidence.

[47] The fast directions observed in the rift valleys and in the diffuse region of block faulting in eastern Tanzania clearly do not match the predicted W–NW direction, even if the measurements had larger error bars, and we can firmly rule out extension-induced LPO of olivine in the lithosphere as the dominant causative mechanism for anisotropy here.

4.2. Anisotropy Due to Parallel Dikes or Magma-Filled Lenses

[48] A preferred orientation of cracks, faults, fractures, or tabular intrusions makes an otherwise homogeneous medium effectively anisotropic for wavelengths much larger than the spacing of the parallel structures [*Backus*, 1962]. When these structures are vertical, the fast direction is parallel to the strike of the structures, and *dt* is proportional to the volume fraction of and velocity contrast across the structures. Because cracks, faults, and fractures are confined to the brittle upper crust (0–15 km), the *dt* associated with such aligned structures are probably within the noise of teleseismic shear wave splitting. This is consistent with the typically observed crustal *dt* of 0.1–0.3 s [*Booth et al.*, 1985, 1990; *Kaneshima et al.*, 1988; *Kaneshima*, 1990; *Shih and Meyer*, 1990; *Crampin*, 1994; *McNamara et al.*, 1994]. However, partially molten tabular intrusions (dikes) are a possible cause of teleseismic splitting because the velocity contrast between magma and the surrounding rock is large, and parallel dikes could penetrate through the entire lithosphere, leading to considerable *dt*.

[49] A shape-preferred orientation (SPO) of vertically oriented water-filled [*Crampin*, 1991] or magma-filled [*Kendall*, 1994] lenses can also lead to effective anisotropy and splitting where ϕ is parallel to the strike of the lenses. Kendall showed that *dt* due to this SPO could be on the order of seconds for some models of partial melt regions beneath mid-ocean ridges.

[50] Because parallel dikes or magma-filled lenses would be a result of partial melt collecting along planes that are perpendicular to the least principal stress direction (σ_3), this hypothesis predicts that station fast directions would be parallel to the current MHCS if there was a steady state active source of partial melt in the asthenospheric mantle and the region of partial melt was currently in a normal-faulting stress state (σ_2 equal to MHCS and σ_1 equal to vertical). Predicted *dt* would be the highest in the center of the rift and would decrease away from the rift because of freezing of the dikes/magma lenses over time. This rate at which *dt* decreases would be (roughly) inversely proportional to the extension strain rate.

[51] *Gao et al.* [1997] favored an interpretation of splitting across the KRISP network in Kenya wherein ϕ resulted from magma-filled lenses striking in the direction parallel to MHCS. Our data set allows a more spatially comprehensive study of splitting in Kenya and Tanzania, and we find some evidence for splitting parallel to MHCS in our off-craton station fast directions but not enough to conclude that either parallel dikes or magma-filled lenses are the dominant

causative mechanism of anisotropy (Figure 9). The fast directions at MBAR and GOMA are parallel and subparallel with MHCS. Fast directions in Kenya north of ~1.0°S are subparallel to the MHCS, but others in Kenya are up to 65° away (e.g., NAI). All fast directions to the south of the craton are ~60° away from MHCS.

[52] The *dt* for the Kenya Rift stations that have MHCS-parallel fast directions are similar to the *dt* for GOMA (adjacent to the Western Rift). However, only Kenya is experiencing considerable volcanism. If aligned magma-filled lenses are responsible for MHCS-parallel fast directions for stations in the Western and Eastern Rifts, one would expect the delay times in the West Rift to be smaller because the magma-filled lenses do not intrude the entire lithosphere as they do beneath the Eastern Rift. We suggest that magma-filled lenses could be contributing to some of the fast directions we observe (e.g., beneath the KRISP network), but it is not the dominant source of anisotropy.

4.3. Fossilized Anisotropy in the Lithosphere

4.3.1. Tanzania Craton

[53] Many active mountain belts today have fast directions that are perpendicular to the direction of shortening [*Silver and Chan*, 1991; *Vinnik et al.*, 1992]. Regions of strike-slip faulting or shear have one or more layers of anisotropy with ϕ parallel to the strike of the structures [*Savage and Silver*, 1993; *Barruol and Hoffman*, 1999; *Audoine et al.*, 2000]. Because temperatures required to significantly modify a lattice preferred orientation of olivine under typical deviatoric stresses are generally thought to be higher than those found throughout the lithosphere [*Vauchez et al.*, 1999], it is probable that ϕ in cratons reflect paleoshortening directions that were fossilized during subsequent lithospheric cooling. If such anisotropy is vertically coherent, then ϕ should be parallel to the geologic structural trends observed in surface outcrops. Where cratons have been modified by multiple orogenic events, one might expect to observe vertically incoherent anisotropy and inconsistent splitting. For the Canadian craton, ϕ is subparallel to the geologic structural trends exposed at the surface, and correlation of increasing *dt* with increasing lithospheric thickness for the Canadian craton can be explained well by fossilized, vertically coherent lithospheric anisotropy [*Silver and Chan*, 1988, 1991]. Splitting observed on the Kaapvaal [*Silver et al.*, 2001; *Fouch et al.*, 2004] and South American cratons [*James and Assumpção*, 1996] has also been interpreted to represent the effects of fossilized anisotropy. The Australian [*Clitheroe and van der Hilst*, 1998] and east European [*Wylegalla et al.*, 1999] cratons and parts of the Siberian [*Gao et al.*, 1997] craton demonstrate small, inconsistent, or no splitting.

[54] Similar to that found for South Africa [*Silver et al.*, 2001; *Fouch et al.*, 2004], we find good evidence of fossilized lithospheric anisotropy in the Tanzania craton. Figure 8 shows a good correlation between some of the on-craton ϕ and the geologic structural trends. In addition, the inconsistent splitting (Figure 4), high proportion of observed ucons for most of the on-craton stations (Figure 5), and rapid change in station estimates between some stations (Figure 8) suggest the presence of lithospheric anisotropy that is somewhat laterally and vertically incoherent. At MBWE the incoherence is so large that the station stack is a ucon result. However, the well-constrained splitting estimates are significantly different from the structural trends for stations URAM in the west; KR42, BARI, TALE, and KAKA in the north; and TUND and PAND in the south (Figures 4 and 8). This suggests a different or additional source of anisotropy.

[55] There is evidence for lithosphere/asthenosphere anisotropy beneath the craton. Surface waves recorded on the Tanzania Network show evidence for small azimuthal anisotropy (~0.8%) with an average NNW ϕ between 80- and 300-km depth, possibly extending up to the base of the crust [*Weeraratne et al.*, 2003]. Although surface waves have poor spatial resolution compared to subvertically incident body waves, ϕ for periods between 20 and 140 s is on average NNW/SSE. This direction is roughly parallel to the splitting ϕ. Using the *dt* equation, Weeraratne et al.'s results predict $dt = 0.4$ s, which is close to the average observed on-craton *dt* (~0.5 s). Defining the base of the lithosphere to be the depth to the center of the maximum negative shear wave velocity gradient, *Weeraratne et al.* [2003] estimate that the lithospheric thickness is ~170 km beneath the craton. Consequently, the surface waves suggest the depth of splitting and anisotropy is in the lithosphere and asthenosphere, suggesting two possible sources of anisotropy.

4.3.2. Mobile Belts and Rifts

[56] Four paleo-orogenic belts surround the Tanzania craton and their associated structural trends are roughly parallel to the edges of the craton (Figure 8). Off-craton ϕ are therefore in good agreement with that predicted by the fossilized anisotropy hypothesis, especially east of the craton. Furthermore, *dt* in eastern Tanzania are short and increase (along with the consistency of splitting) away from the rift toward the Indian Ocean in the direction of presumably thicker lithosphere. However, the considerable *dt* for other off-craton stations suggests that the majority of the anisotropy is not located in the lithosphere. For example, the lithospheric mantle thickness beneath the Kenya Rift is only ~50 km thick [*Green et al.*, 1991; *Achauer et al.*, 1994; *Slack et al.*, 1994] but is generally thought to thicken toward the south into eastern Tanzania. Yet the longest *dt* in the study area is observed in Kenya, and *dt* decrease toward the south into Tanzania. To quantify this point using the *dt* equation, a bulk *S* wave anisotropy of ~4% (a commonly found value for deformed dunites [e.g., *Mainprice and Silver*, 1993; *Kern et al.*, 1996]) and the ~50-km-thick mantle beneath the Kenya Rift predict a $dt = 0.5$ s. However, the *dt* in Kenya is more than twice as long ($dt = 1.2$ s). Similarly, in the Western Rift (station GOMA) the mantle lithosphere may be only ~20 km thick [*Nolet and Mueller*, 1982], yet the consistent rift-parallel splitting has $dt = 1.0$ s. In summary, it is probable that fossil anisotropy is contributing to the observed splitting patterns considering the rapid changes observed over short distances in some places, but the large *dt* in the rift and the rift *dt* gradient from south to north argues against this being the dominant source of anisotropy.

4.4. Active Shear at the Base of the Plate

4.4.1. Asthenospheric Flow

[57] Lattice preferred orientations of the fast [100] *a* axes of olivine probably develop in the asthenosphere because of

dislocation-creep deformation associated with simple shear at the base of the plate [e.g., *Nicolas*, 1989; *Zhang and Karato*, 1995; *Tommasi et al.*, 1996; *Tommasi*, 1998]. These orientations are roughly horizontal and in the direction of shear. Consequently, simple asthenospheric flow due to the passive shearing of the asthenosphere by the moving plate has been invoked to interpret ϕ parallel to absolute plate motion (APM) [*Silver and Chan*, 1991; *Vinnik et al.*, 1992; *Bormann et al.*, 1993; *Russo and Okal*, 1998; *Wolfe and Silver*, 1998; *Schutt et al.*, 1998; *Wolfe and Solomon*, 1998]. Where *dt* are longer than that which can be reasonably explained by lithospheric anisotropy, adding an additional free parameter allows one to explain any ϕ as a result of relative motion between a separately moving plate and asthenosphere [*Silver and Holt*, 2002; *Gök et al.*, 2003]. These versions of the asthenospheric flow hypothesis assume there is no significant topography along the lithosphere/asthenosphere boundary.

[58] To show regions of lithospheric thinning and upper mantle structure at depth, we overlay the final station estimates upon the results at 200-km depth of an *S* wave tomographic image [*Ritsema et al.*, 1998] (Figure 9). The APM of Africa appears to be slow, and thus it has been a challenge to constrain the direction. Preliminary results suggested a NE direction [*Minster and Jordan*, 1978; *Gripp and Gordon*, 1990], but this has more recently been refined to 285° ± 45° at 15 ± 3 mm/yr [*Gripp and Gordon*, 2002].

[59] Our station fast directions vary throughout the study area (Figure 9) and are therefore not explained by the simple asthenospheric flow hypothesis. However, the average on-craton ϕ is approximately parallel to the WNW APM. These on-craton data are consistent with the asthenospheric flow hypothesis if the plate is moving with respect to the underlying mantle, creating simple shear at the base of the craton.

4.4.2. Asthenospheric Flow With Basal Lithospheric Topography and Plume Flow

[60] If there is relative motion between the lithosphere and the underlying mantle, the asthenosphere must flow around and/or beneath craton keels. *Bormann et al.* [1996] interpreted ϕ in Europe as due to asthenospheric flow associated with basal lithospheric topography. In most regions of gentle topographical gradients, ϕ is parallel to APM [*Gripp and Gordon*, 1990, 2002]. In regions where the topographic gradients are large, ϕ tends to be parallel to the topographic contours of the Moho topography, which are assumed to reflect the same variations in basal lithospheric topography. If the latter assumption is correct, this suggests the asthenosphere is flowing around (rather than beneath) topography along the base of the lithosphere.

[61] *Fouch et al.* [2000] modeled the anisotropy expected for subcontinental mantle flow around a craton keel and found that such a model complicated by additional lithospheric anisotropy may explain shear wave splitting beneath eastern North America as well. Their calculations predict that splitting beneath this or any relatively flat lithospheric keel would have APM-parallel ϕ, whereas splitting elsewhere would have ϕ parallel to the depth contours at the base of the lithosphere because the rigid lithosphere is moving through the asthenosphere. We hereinafter refer to this model as the "edge flow model."

[62] The NNW/SSE fast direction we found for the westernmost on-craton station (URAM) and the E/W fast directions for stations south of the craton are approximately parallel to the craton edge and rift and can be explained by edge flow around the keel and/or rift-parallel flow. As mentioned in section 3.4, the average fast direction for the on-craton stations is NW, which is subparallel to the absolute plate motion direction, and is also predicted by this model.

[63] The edge flow model alone cannot explain splitting along the eastern side of the craton where ϕ are not consistently parallel to the craton edge. However, edge flow would produce an ~N/S fabric, which combined with additional anisotropy at shallower depths could produce the ±35° ϕ variation with *dt* as long as those observed in Kenya (~1.2 s).

[64] Station INZA is a station for which a single-layer horizontal fast azimuth model is not resolvable because events that arrived from easterly back azimuths had E/W ϕ, whereas those from the westerly back azimuths had N/S ϕ (Figure 5 and Figure 1 in auxiliary material). The E/W ϕ is subparallel to APM and argues for a zone of simple asthenospheric flow just to the east of INZA. If the edge flow model is correct, somewhere between this zone and station URAM (western craton) is the onset of edge flow around the craton keel. In addition, splitting complexity observed immediately east of the craton, which disappears farther east beneath station HALE, can be explained by a keel sheltering effect the keel has on the asthenosphere to the east. This sheltering effect could give rise to either asthenospheric stagnation if flow is laminar and there is no N/S edge flow. However, if the flow is turbulent, this would most likely be a region of localized convection associated with upwelling asthenosphere in the wake of the WNW moving craton in a fashion similar to that found by *King and Anderson* [1998], although their modeling assumed that the convection was driven by thermal instabilities associated with conductive insulation by the craton. Although we feel this latter situation is physically plausible, we recognize that it was not predicted by the modeling results of *Fouch et al.* [2000].

4.4.3. Plume Models and Rift-Parallel Flow

[65] The mantle plume hypothesis predicts that ascending plume material is deflected by the lithosphere, which could lead to the development of an olivine LPO and bulk anisotropy. Thus an essential part of the plume hypothesis, the deflection of plume material, can be tested by measurements of mantle anisotropy [*Savage and Sheehan*, 2000]. *Walker et al.* [2001, 2003] showed that the kinematics of lateral flow expected for a simple Hawaiian plume model is consistent with fast directions on the few seismic stations around Hawaii for which broadband seismic data are publicly available. However, the predictions of that model did not deviate very much from the predictions due to simple asthenospheric flow. Splitting fast directions recorded on a much larger data set around the Eifel hotspot are also predicted by a simple plume model (K. T. Walker et al., Shear-wave splitting around the Eifel hotspot: Evidence for plume-related flow, submitted to *Geophysical Journal International*, 2003). However, basal shear associated with a plume does not predict splitting around the Iceland [*Bjarnason et al.*, 2002] hotspot. The Yellowstone

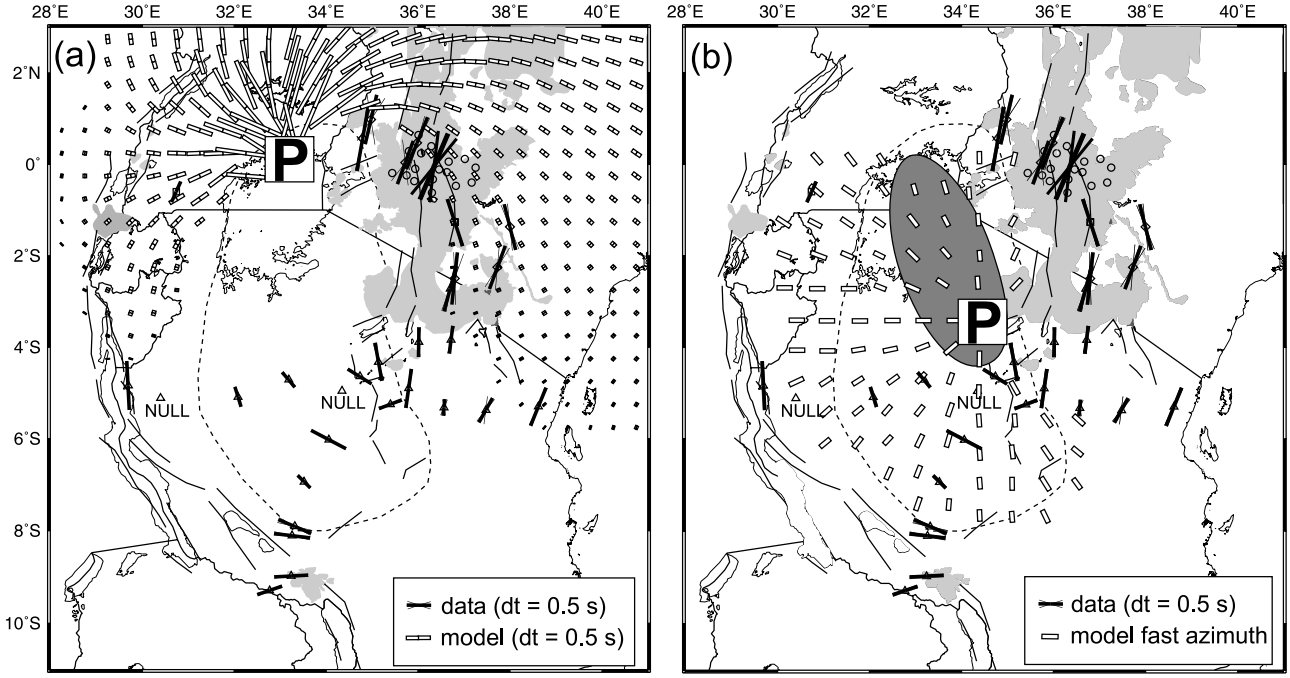

Figure 10. Testing models of upper mantle flow beneath the East African Plateau. We compare our station estimates (solid) with fast direction predictions (open) by (a) *Sleep et al.* [2002], who used numerical modeling to simulate asthenospheric flow for a single plume (P) beneath southeastern Uganda, and (b) *Weeraratne et al.* [2003], who inverted surface wave dispersion curves recorded across the Tanzania Network for the best fitting radial fast azimuth pattern due to a single plume (P, dark shading indicates 95% confidence region). The lengths of the model fast directions are proportional to the associated delay times in Figure 10a and normalized to unity in Figure 10b.

(R. Smith, personal communication, 2004) and Society (G. Barruol, personal communication, 2004) hotspots are being investigated.

[66] Owing to a rich history of various directions and magnitudes of extension in eastern Africa, there are likely to be channels in the base of the lithosphere (e.g., NW striking Anza graben in Kenya) that could guide plume-related flow. *Sandvol et al.* [1992] analyzed splitting in the Rio Grande Rift and found ϕ to be subparallel to the rift, which they interpreted to be due to channeled asthenospheric flow at the base of the lithosphere. On the basis of new *P* wave residual and gravity data showing a wide zone of lithospheric thinning, *Gao et al.* [2003] have recently reconsidered their shear wave splitting for the Baikal Rift to be due to localized convection beneath the rift.

[67] Figure 10 compares our splitting estimates with those predicted for two different plume models. A plume has been proposed to exist beneath the East African Plateau to explain the high elevations, magmatism, and low seismic velocity at the base of the Tanzania craton [*Ebinger et al.*, 1989; *Simiyu and Keller*, 1997; *Nyblade et al.*, 2000]. Using an estimate of Eocene East Africa lithospheric variations, *Ebinger and Sleep* [1998] calculated the lateral asthenospheric flow expected for a single plume located beneath Ethiopia. Their model explains the distribution and timing of magmatism and uplift throughout much of East Africa if a thin lithosphere beneath the Eastern and Western Rifts channels the flow. Introducing the effects of craton keels into their simulations, *Sleep et al.* [2002] modeled the lateral flow for a plume located beneath the northern edge of the Tanzania craton and calculated the expected splitting that would be observed (Figure 10a). The predicted plume material flows around the craton down to a latitude of about 4°S. Although their plume material does not extend far enough south to test their predictions against our Tanzania data, their predicted ϕ are only parallel to our observed ϕ at stations NAI and KMBO. The location of the modeled plume center was selected in an ad hoc manner (M. Kendall, personal communication, 2003). In addition, the included lithospheric thickness variations, which control to a first-order the direction of plume flow, did not include variations due to late Cenozoic rifting. Because the fast-direction predictions are directly controlled by the topography along the base of the plate and because the delay-time predictions are controlled by how far the initial plume head spreads laterally beneath the plate, it appears likely that the plume model would explain most or all of our off-craton splitting data if (1) the plume center of *Sleep et al.* [2002] had been placed farther north beneath Ethiopia as done by *Ebinger and Sleep* [1998], (2) the initial plume head was made larger to allow plume material to spread farther laterally, and (3) the oceanic lithosphere was made thicker than the adjacent continental lithosphere constraining the plume material to flow parallel to the coast (this would be an expected result of late Cenozoic rifting).

[68] *Weeraratne et al.* [2003] inverted Tanzania surface wave phase-velocity data for two azimuthal anisotropy models: a uniform azimuth model and a radial azimuth model. Their uniform model was derived by dividing the region into two model domains: the craton and the sur-

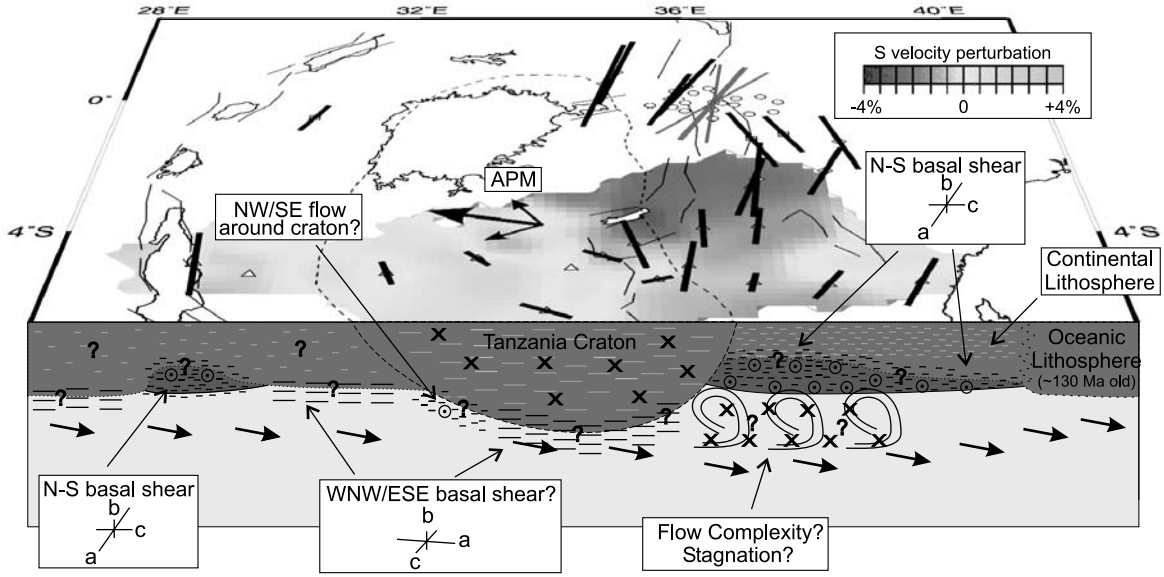

Figure 11. Cross section at 5°S showing possible sources of anisotropy that could explain splitting. Station splitting estimates are shown with delay time scaled to approximately correct for the three-dimensional view. A shear wave velocity tomographic image at 200-km depth is shown at the surface [*Ritsema et al.*, 1998]. The absolute plate motion (APM) is WNW [*Gripp and Gordon*, 2002]. Thin arrows in the asthenosphere (yellow) indicate the flow direction relative to the cratonic lithosphere (blue). Long dashes indicate olivine LPO with ~WNW/ESE fast *a* axes due to shear at the base of the keel (black) and fossilized from past orogenic events (gray). Shorter dashes indicate ~N/S fast *a* axes from plume flow (red) beneath thinned lithosphere and possible corner flow around the keel (black) and fossilized from prior orogenic events (gray). Crosses indicate additional anisotropy from previous orogenic events. Question marks indicate uncertain boundary locations and/or anisotropy. Dots with circles indicate flow is coming out of the page. The depth to the base of the craton is here defined by the 170-km depth to the center of the maximum negative shear wave velocity gradient [*Weeraratne et al.*, 2003]. See color version of this figure at back of this issue.

rounding area. In each domain the anisotropy was allowed to vary only for each period (20–140 s). They performed a grid search to find the optimum model, then prescribed the average NNW direction to all periods in order to calculate the optimum model's variance reduction. For their radial model they assumed that a plume exists beneath the Tanzania craton and gives rise to a radial pattern of azimuthal anisotropy in the lower lithosphere and asthenosphere. They permitted the anisotropy magnitude to vary with period but fixed the fast directions at all periods to be horizontal and radiating away from the plume center. They then performed another grid search to find the optimum plume location. The authors report that their best radial model (Figure 10b) predicts the data better than their best uniform model. However, the uniform model's variance reduction is not based on the full range of the fast directions found in the inversion but on the average. The fit of the full uniform model would fit the data better, but the exact improvement in fit is unclear. Our observed shear wave splitting ϕ are not predicted by their radial model but are roughly predicted by their uniform azimuth model.

5. Synthesis

[69] East Africa is a unique, tectonically complex region owing to the presence of a rigid craton, paleothrust belts and shear zones, active magmatism and rifting, and at least one nearby hotspot. If many different mechanisms that lead to mantle anisotropy exist, complicated splitting in this region would be expected. Consistent with this expectation, we observe inconsistent splitting and a large proportion of unconstrained splitting measurements beneath the craton and in eastern Tanzania. Observations of splitting for different back azimuths suggest lateral variations in anisotropy. Fresnel zone constraints on the maximum depth extent of anisotropy suggest the presence of vertical anisotropy variations. We could not find simple dipping-axis or two-layer models that were consistent between nearby stations, yet we could find many different dipping-axis and two-layer models that fit the data at each station with roughly the same degree of success. Consequently, we interpret the anisotropy beneath each station to be due to minor lateral and vertical variations of a single anisotropic layer with a horizontal fast axis. We generate station splitting estimates (averages) to estimate the parameters of this single-layer model and find good regional consistency that can be explained by several anisotropy-producing mechanisms.

[70] Figure 11 is an E–W cross section showing our tectonic/geodynamic interpretation. The observed off-craton ϕ throughout the study area are subparallel to the nearby rifts, craton edges, geologic structural trends, and recent most horizontal compressive stress direction. Splitting beneath the craton has ϕ subparallel to the structural trends at the surface and absolute plate motion [*Gripp and Gordon*,

2002]. Both splitting ϕ and surface wave azimuthal anisotropy results suggest azimuthal anisotropy in the lithosphere and asthenosphere from 300-km depth up to at least 80 km and possibly to the base of the crust. At station INZA, $\sim$N/S ϕ occur for westerly events, and $\sim$E/W ϕ occur for easterly events (Figure 5). The region southeast of the craton in Tanzania is characterized by inconsistent splitting and many observed ucons (Figures 4 and 5). The considerable 1.2-s *dt* observed for Kenya stations and the decrease in *dt* from $\sim$80-km-thick lithosphere in Kenya toward thicker lithosphere in the south in Tanzania suggest that at least part of the anisotropy here must exist in the asthenosphere. These observations suggest that splitting is most likely caused by an olivine LPO due to shear along the base of the lithosphere associated with (1) normal asthenosphere that is flowing around the craton keel in response to west-northwest plate motion through the asthenosphere [*Fouch et al.*, 2000] and/or (2) plume material guided by channels of thinned lithosphere [*Sleep et al.*, 2002]. Significant ϕ variation between nearby stations in some places (up to 65°) suggests the presence of shallow anisotropy. The upper layer of anisotropy in a medium of slowly varying anisotropy [*Rümpker and Silver*, 1998] or two-layer anisotropy [*Saltzer et al.*, 2000] has the strongest effect on the final station splitting estimates. We therefore suggest that the observed variations are due to the subtle complexity (which we could not model sufficiently) introduced by domains of fossilized anisotropy and/or concentrations of aligned magma lenses or partially molten dikes in the lithosphere but that the main source of anisotropy is in the asthenosphere.

[71] Patterns observed in the delays of teleseismic *S* and *P* waves [*Bokelmann and Silver*, 2000; *Bokelmann*, 2002a], shear wave splitting [*Silver and Kaneshima*, 1993] and surface wave studies [*Babuška et al.*, 1998] on stations located around and across the Canadian craton suggest the presence of anisotropy at the base of the craton keel, with a horizontal fabric implying shear between the plate and underlying mantle [*Bokelmann*, 2002b]. The geometry of this anisotropy as resolved by teleseismic *P* waves for interior craton stations suggests fast axes dipping toward the APM direction. These studies suggest that the lower keel is being sheared because of traction between it and the underlying mantle and that the horizontal motion of the underlying mantle is faster than the lithosphere, implying that convection currents in the mantle contribute to (if not drive completely) plate tectonics. Splitting observations across the Tanzania craton do not show evidence for a consistently dipping fast axis (Figure 7a).

[72] The most robust conclusion of this study is that there is no evidence from shear wave splitting for ductile thinning of the lithospheric mantle via dislocation creep; that is, extension-induced LPO anisotropy is not a dominant cause of anisotropy in East Africa, at least as far south along the rift as Kenya and Tanzania. This is surprising given the long history of extension in the region and suggests that extension in East Africa occurs via magmatic intrusion (diking) or via ductile thinning within very narrow rift zones. Given the good evidence for fossilized anisotropy in the lithosphere beneath the off-craton stations, we speculate that the fossilized N/S fabrics may have imparted a mechanical anisotropy to the lithosphere, allowing relatively small extensional stresses to rift the East African lithosphere without the generation of an olivine LPO [*Vauchez et al.*, 1997] despite the addition of elevated mantle temperatures beneath the East African Plateau.

[73] **Acknowledgments.** We are thank S. Simiyu for field assistance in Kenya and C. Moshy, P. Ngereja, and A. Tesha for field assistance in Tanzania. We also thank G. Helffrich and P. Silver for providing their splitting code, which we modified and converted to C++ for this research, R. Gordon for providing code to calculate standard errors for the HS3-NUVEL1A plate motion model, M. Kendall for providing splitting predictions, and A. Sebai for sharing her African surface-wave anisotropy results. IRIS DMC provided waveform and metadata. The DMC BREQFAST request system greatly facilitates shear wave splitting research. The USGS Albuquerque Seismological Laboratory and SIO acquired the GSN waveform data, ANSS provided online access to earthquake hypocenter locations, and the 2000 World Stress Map Project provided stress data. We used GMT software [*Wessel and Smith*, 1991] to prepare figures and SAC2000 (Lawrence Livermore National Laboratory, University of California) for basic seismic data processing. We thank P. Goldstein and G. Helffrich for providing assistance with SAC2000. Finally, we thank M. Savage, M. Fouch, and E. Garnero for provided constructive comments that improved this paper. This work was supported by the National Science Foundation (EAR 930455, 9903093, and 0003424).

References

Achauer, U., and the KRISP Teleseismic Working Group (1994), New ideas of the Kenya rift based on the inversion of the combined dataset of the 1985 and 1989/90 seismic tomography experiments, *Tectonophysics*, *236*, 305–330.

Alsina, D., and R. Snieder (1995), Small-scale sublithospheric continental margin deformation: Constraints from SKS splitting observations, *Geophys. J. Int.*, *123*, 4313–4448.

Audoine, E., M. K. Savage, and K. Gledhill (2000), Seismic anisotropy from local earthquakes in the transition region from a subduction to a strike-slip plate boundary, New Zealand, *J. Geophys. Res.*, *105*, 8013–8033.

Babuška, V. J., J. Plomerová, and J. Sileny (1993), Models of seismic anisotropy in the deep continental lithosphere, *Phys. Earth Planet. Inter.*, *78*, 167–191.

Babuška, V., J. P. Montagner, J. Plomerová, and N. Girardin (1998), Age-dependent large-scale fabric of the mantle lithosphere as derived from surface-wave velocity anisotropy, in *Geodynamics of Lithosphere and Earth's Mantle: Seismic Anisotropy as a Record of Past and Present Dynamic Processes*, edited by R. C. Liebermann and V. Babuška, *Pure. Appl. Geophys.*, *151*, 257–280.

Backus, G. E. (1962), Long-wave elastic anisotropy produced by horizontal layering, *J. Geophys. Res.*, *67*, 4427–4440.

Barruol, G., and R. Hoffman (1999), Upper mantle anisotropy beneath the Geoscope stations, *J. Geophys. Res.*, *104*, 10,757–10,773.

Barruol, G., and W. B. Ismail (2001), Upper mantle anisotropy beneath the African IRIS and Geoscope stations, *Geophys. J. Int.*, *146*, 549–561.

Bjarnason, I. T., P. G. Silver, G. Rümpker, and S. C. Solomon (2002), Shear wave splitting across the Iceland hot spot: Results from the ICEMELT experiment, *J. Geophys. Res.*, *107*(B12), 2382, doi:10.1029/2001JB000916.

Bokelmann, G. H. R. (2002a), Convection-driven motion of North America craton: Evidence from *P*-wave anisotropy, *Geophys. J. Int.*, *148*, 278–287.

Bokelmann, G. H. R. (2002b), Which forces drive North America?, *Geology*, *30*, 1027–1030.

Bokelmann, G. H. R., and P. G. Silver (2000), Mantle variation within the Canadian Shield: Travel times from the portable broadband Archean-Proterozoic Transect 1989, *J. Geophys. Res.*, *105*, 579–605.

Booth, D. C., S. Crampin, R. Evans, and G. Roberts (1985), Shear-wave polarizations near the North Anatolian Fault-I. Evidence for anisotropy-induced shear-wave splitting, *Geophys. J. R. Astron. Soc.*, *83*, 61–73.

Booth, D. C., S. Crampin, J. H. Lovell, and J.-M. Chiu (1990), Temporal changes in shear wave splitting during an earthquake swarm in Arkansas, *J. Geophys. Res.*, *95*, 11,151–11,164.

Bormann, P., P.-T. Burghardt, L. I. Makeyeva, and L. P. Vinnik (1993), Teleseismic shear-wave splitting and deformations in central Europe, *Phys. Earth Planet. Inter.*, *78*, 157–166.

Bormann, P., G. Grünthal, R. Kind, and H. Montag (1996), Upper mantle anisotropy beneath central Europe from *SKS* wave splitting: Effects of absolute plate motion and lithosphere-asthenosphere boundary topography?, *J. Geodyn.*, *22*, 11–32.

Bosworth, W., M. R. Strecker, and P. M. Blisniuk (1992), Integration of East African paleostress and present-day stress data: Implications for continental stress field dynamics, *J. Geophys. Res.*, *97*, 11,851–11,865.

Brazier, R. A., A. A. Nyblade, C. A. Langston, and T. J. Owens (2000), *Pn* wave velocities beneath the Tanzania craton and adjacent rifted mobile belts, East Africa, *Geophys. Res. Lett.*, *27*, 2365–2368.

Burnham, K. P., and D. R. Anderson (2002), *Model Selection and Multimodel Inference: A Practical Information-Theoretical Approach*, 488 pp., Springer-Verlag, New York.

Cahen, L., N. J. Snelling, J. Delhal, and J. R. Vail (1984), *The Geochronology and Evolution of Africa*, 512 pp., Oxford Univ. Press, New York.

Chevrot, S., and R. D. van der Hilst (2003), On the effects of a dipping axis of symmetry on shear-wave splitting measurements in a transversely isotropic medium, *Geophys. J. Int.*, *152*, 497–505.

Christensen, N. I. (1966), Shear wave velocities in metamorphic rocks at pressures to 10 kilobars, *J. Geophys. Res.*, *71*, 3549–3556.

Christensen, N. I. (1984), The magnitude, symmetry, and origin of upper mantle anisotropy based on fabric analysis of ultramafic tectonites, *Geophys. J. R. Astron. Soc.*, *76*, 89–111.

Clitheroe, G., and R. van der Hilst (1998), Complex anisotropy in the Australian lithosphere from shear-wave splitting in broad-band *SKS* records, in *Structure and Evolution of the Australian Continent*, *Geodyn. Ser.*, edited by J. Braun et al., vol. 26, pp. 73–78, AGU, Washington D. C.

Crampin, S. (1991), Wave propagation through fluid-filled inclusions of various shapes: Interpretation of extensive-dilatancy anisotropy, *Geophys. J. Int.*, *104*, 611–623.

Crampin, S. (1994), The fracture criticality of crustal rocks, *Geophys. J. Int.*, *118*, 428–438.

Dawson, J. B. (1992), Neogene tectonics and volcanicity in the north Tanzania sector of the Gregory rift valley: Contrasts with the Kenya sector, *Tectonophysics*, *204*, 81–92.

Ebinger, C. J., and N. H. Sleep (1998), Cenozoic magmatism throughout east Africa resulting from impact of a single plume, *Nature*, *395*, 788–791.

Ebinger, C. J., T. D. Bechtel, D. W. Forsyth, and C. O. Bowin (1989), Effective elastic plate thickness beneath the East African and Afar plateaus and dynamic compensation of the uplifts, *J. Geophys. Res.*, *94*, 2883–2901.

Ebinger, C. J., Y. Poudjom, E. Mbede, F. Foster, and J. B. Dawson (1997), Rifting Archean lithosphere: The Eyasi-Manyara-Natron rifts, East Africa, *J. Geol. Soc. London*, *154*, 947–960.

Foster, A., C. Ebinger, E. Mbede, and D. Rex (1997), Tectonic development of the northern Tanzanian sector of the East African rift system, *J. Geol. Soc. London*, *154*, 689–700.

Fouch, M. J., and K. M. Fischer (1996), Mantle anisotropy beneath northwest Pacific subduction zones, *J. Geophys. Res.*, *101*, 15,987–16,002.

Fouch, M. J., K. M. Fischer, E. M. Parmentier, M. E. Wysession, and T. J. Clarke (2000), Shear-wave splitting, continental keels, and patterns of mantle flow, *J. Geophys. Res.*, *105*, 6255–6275.

Fouch, M. J., P. G. Silver, D. R. Bell, and J. N. Lee (2004), Small-scale variations in seismic anisotropy near Kimberley, South Africa, *Geophys. J. Int.*, *157*, 764–774, doi:10.1111/j.1365-246X.2004.02234.x.

Fuchs, K., B. Altherr, B. Muller, and C. Prodehl (1997), Structure and dynamic processes in the lithosphere of the Afro-Arabian rift system, *Tectonophysics*, *278*, 1–352.

Gao, S., P. M. Davis, H. Liu, P. D. Slack, A. W. Rigor, Y. A. Zorin, V. V. Mordvinova, V. M. Kozhevnikov, and N. A. Logatchev (1997), *SKS* splitting beneath continental rift zones, *J. Geophys. Res.*, *102*, 22,781–22,797.

Gao, S. S., K. H. Liu, P. M. Davis, P. D. Slack, Y. A. Zorin, V. V. Mordvinova, and V. M. Kozhevnikov (2003), Evidence for small-scale mantle convection in the upper mantle beneath the Baikal rift zone, *J. Geophys. Res.*, *108*(B4), 2194, doi:10.1029/2002JB002039.

Gök, R., J. F. Ni, M. West, E. Sandvol, D. Wilson, R. Aster, W. S. Baldridge, S. Grand, W. Gao, F. Tillman, and S. Semken (2003), Shear wave splitting and mantle flow beneath LA RISTRA, *Geophys. Res. Lett.*, *30*(12), 1614, doi:10.1029/2002GL016616.

Green, W. V., U. Achauer, and R. P. Meyer (1991), A three-dimensional seismic image of the crust and upper mantle beneath the Kenya rift, *Nature*, *354*, 199–203.

Gripp, A. E., and R. G. Gordon (1990), Current plate velocities relative to the hotspots incorporating the NUVEL-1 global plate motion model, *Geophys. Res. Lett.*, *17*, 1109–1112.

Gripp, A. E., and R. G. Gordon (2002), Young tracks of hotspots and current plate velocities, *Geophys. J. Int.*, *150*, 321–361.

Hartog, R., and S. Y. Schwartz (2000), Subduction-induced strain in the upper mantle east of the Mendocino triple junction, California, *J. Geophys. Res.*, *105*, 7909–7930.

Haug, G. H., and M. R. Strecker (1995), Volcano-tectonic evolution of the Chyulu Hills and implications for the regional stress field in Kenya, *Geology*, *23*, 165–168.

Holmes, A. (1951), The sequence of Pre-Cambrian orogenic belts in south and central Africa, *Proc. 18 Int. Geol. Congr.*, *14*, 254–269.

James, D. E., and M. Assumpção (1996), Tectonic implications of *S*-wave anisotropy beneath SE Brazil, *Geophys. J. Int.*, *126*, 1–10.

Jenkins, G., and D. Watts (1969), *Spectral Analysis and Its Applications*, 138 pp., Holden-Day, Boca Raton, Fla.

Kaneshima, S. (1990), Origin of crustal anisotropy: Shear wave splitting studies in Japan, *J. Geophys. Res.*, *95*, 11,121–11,133.

Kaneshima, S., M. Ando, and S. Kimura (1988), Evidence from shear-wave splitting for the restriction of seismic anisotropy to the upper crust, *Nature*, *335*, 627–629.

Karato, S. (1989), Seismic anisotropy: Mechanisms and tectonic implications, in *Rheology of Solids and of the Earth*, edited by S. Karato and M. Toriumi, pp. 393–422, Oxford Univ. Press, New York.

Kendall, J.-M. (1994), Teleseismic arrivals at a mid-ocean ridge: Effects of mantle melt and anisotropy, *Geophys. Res. Lett.*, *21*, 301–304.

Kendall, J.-M. (2000), Seismic anisotropy in the boundary layers of the mantle, in *Earth's Deep Interior: Mineral Physics and Tomography From Atomic to the Global Scale*, edited by S. Karato et al., *Geophys. Monogr. Ser.*, vol. 117, pp. 149–175, AGU, Washington, D. C.

Kern, H., L. Burlini, and I. V. Ashchepkov (1996), Fabric-related seismic anisotropy in upper-mantle xenoliths: Evidence from measurements and calculations, *Physics Earth Planet. Inter.*, *95*, 195–209.

Key, R. M., T. J. Charsley, B. Hackman, A. F. Wilkinson, and C. C. Rundle (1989), Superimposed upper Proterozoic collision controlled orogenesis in the Mozambique orogenic belt of Kenya, *Precambrian Res.*, *44*, 197–225.

King, S. D., and D. L. Anderson (1998), Edge-driven convection, *Earth Planet. Sci. Lett.*, *160*, 289–296.

Kumazawa, M., and O. L. Anderson (1969), Elastic moduli, pressure derivatives, and temperature derivatives of single-crystal olivine and single-crystal forsterite, *J. Geophys. Res.*, *74*, 5961–5972.

Last, R. J., A. A. Nyblade, C. A. Langston, and T. J. Owens (1997), Crustal structure of the East African plateau from receiver functions and Rayleigh wave phase velocities, *J. Geophys. Res.*, *102*, 24,469–24,483.

Lenoir, J. L., J. P. Liegeois, K. Theunissen, and J. Klerkx (1994), The Paleoproterozoic Ubendian shear belt in Tanzania: Geochronology and structure, *J. Afr. Earth Sci.*, *19*, 160–184.

Mainprice, D., and P. G. Silver (1993), Interpretation of *SKS*-waves using samples from the subcontinental lithosphere, *Phys. Earth Planet. Inter.*, *78*, 257–280.

McKenzie, D. (1979), Finite deformation during fluid flow, *Geophys. J. R. Astron. Soc.*, *99*, 13,655–13,665.

McNamara, D. E., T. J. Owens, P. G. Silver, and F. T. Wu (1994), Shear wave anisotropy beneath the Tibetan Plateau, *J. Geophys. Res.*, *99*, 13,655–13,665.

Minster, J. B., and T. H. Jordan (1978), Present-day plate motions, *J. Geophys. Res.*, *83*, 5331–5354.

Montagner, J.-P. (1994), What can seismology tell us about mantle convection?, *Rev. Geophys.*, *32*, 115–137.

Montagner, J. P., and L. Guillot (2000), Seismic anisotropy in the Earth's Mantle, in *Problems in Geophysics for the Next Millenium*, edited by E. Boschi et al., pp. 218–253, Ed. Compostri, Bologna, Italy.

Nicolas, A. (1989), *Structures of Ophiolites and Dynamics of Oceanic Lithosphere*, 367 pp., Kluwer Acad., Norwell, Mass.

Nicolas, A., and N. I. Christensen (1987), Formation of anisotropy in upper mantle peridotites—A review, in *Composition, Structure and Dynamics of the Lithosphere-Asthenosphere System*, edited by K. Fuchs and C. Froidevaux, *Geodyn. Ser.*, vol. 16, pp. 111–123, AGU, Washington D. C.

Nicolas, A., and J. P. Poirier (1976), *Crystalline Plasticity and Solid State Flow in Metamorphic Rocks*, 444 pp., John Wiley, New York.

Noble, W. P., D. A. Foster, and A. J. W. Gleadow (1997), The post-Pan-African thermal and extensional history of crystalline basement rocks in eastern Tanzania, *Tectonophysics*, *275*, 331–350.

Nolet, G., and S. Mueller (1982), A model for the deep structure of the East African rift system from the simultaneous inversion of teleseismic data, *Tectonophysics*, *84*, 151–178.

Nyblade, A. A. (2002), Crust and upper mantle structure in East Africa: Implications for the origin of Cenozoic rifting and volcanism and the formation of magmatic rifted margins, in *Volcanic Rifted Margins*, edited by M. A. Menzies et al., *Spec. Pap. Geol. Soc. Am.*, *362*, 15–26.

Nyblade, A. A., and R. A. Brazier (2002), Precambrian lithospheric controls on the development of the East African rift system, *Geology*, *30*, 755–758.

Nyblade, A. A., and C. A. Langston (2002), Broadband seismic experiments probe the East African rift, *Eos Trans. AGU*, *83*, 405, 407–408.

Nyblade, A. A., and S. W. Robinson (1994), The African superswell, *Geophys. Res. Lett.*, *21*, 765–768.

Nyblade, A. A., C. Birt, C. A. Langston, T. J. Owens, and R. J. Last (1996), Seismic experiment reveals rifting of craton in Tanzania, *Eos Trans. AGU*, *77*, 517, 521.

Nyblade, A. A., T. J. Owens, H. Gurrola, J. Ritsema, and C. A. Langston (2000), Seismic evidence for a deep upper mantle thermal anomaly beneath east Africa, *Geology*, *28*, 599–602.

Owens, T. J., A. A. Nyblade, H. Gurrola, and C. A. Langston (2000), Mantle transition zone structure beneath Tanzania, East Africa, *Geophys. Res. Lett.*, *27*, 827–830.

Prodehl, C., G. R. Keller, and M. A. Khan (1994), Crustal and upper mantle structure of the Kenya Rift, *Tectonophysics*, *236*, 1–483.

Ribe, N. (1992), On the relation between seismic anisotropy and finite strain, *J. Geophys. Res.*, *97*, 8737–8747.

Ribe, N., and Y. Yu (1991), A theory for plastic deformation and textural evolution of olivine polycrystals, *J. Geophys. Res.*, *96*, 8325–8335.

Ritsema, J., A. A. Nyblade, T. J. Owens, and C. A. Langston (1998), Upper mantle seismic velocity structure beneath Tanzania, East Africa: Implications for the stability of cratonic lithosphere, *J. Geophys. Res.*, *103*, 21,201–21,213.

Rümpker, G., and T. Ryberg (2000), New Fresnel-zone estimates for shear-wave splitting observations from finite-difference modeling, *Geophys. Res. Lett.*, *27*, 2005–2008.

Rümpker, G., and P. G. Silver (1998), Apparent shear-wave splitting parameters in the presence of vertically varying anisotropy, *Geophys. J. Int.*, *135*, 790–800.

Russo, R. M., and E. A. Okal (1998), Shear wave splitting and upper mantle deformation in French Polynesia: Evidence for small-scale heterogeneity related to the Society hotspot, *J. Geophys. Res.*, *103*, 15,089–15,107.

Saltzer, R. L., J. B. Gaherty, and T. H. Jordan (2000), How are vertical shear wave splitting measurements affected by variations in the orientation of azimuthal anisotropy with depth?, *Geophys. J. Int.*, *141*, 374–390.

Sandvol, E., J. Ni, S. Ozalaybey, and J. Schlue (1992), Shear-wave splitting in the Rio Grande Rift, *Geophys. Res. Lett.*, *19*, 2337–2340.

Savage, M. K. (1999), Seismic anisotropy and mantle deformation: What have we learned from shear wave splitting?, *Rev. Geophys.*, *37*, 65–106.

Savage, M. K., and A. F. Sheehan (2000), Seismic anisotropy and mantle flow from the Great Basin to the Great Plains, western United States, *J. Geophys. Res.*, *105*, 13,715–13,734.

Savage, M. K., and P. G. Silver (1993), Mantle deformation and tectonics: Constraints from seismic anisotropy in the western United States, *Phys. Earth Planet. Inter.*, *78*, 207–227.

Schutt, D., E. D. Humphreys, and K. Dueker (1998), Anisotropy of the Yellowstone Hot Spot wake, eastern Snake River Plain, Idaho, *Pure Appl. Geophys.*, *151*, 443–462.

Shackleton, R. M. (1986), Precambrian collision tectonics in Africa, in *Collision Tectonics*, edited by M. P. Coward and A. C. Ries, *Geol. Soc. Spec. Publ.*, *19*, 329–349.

Shih, X. R., and R. P. Meyer (1990), Observation of shear wave splitting from natural events: South moat of Long Valley Caldera, California, June 29 to August 12, 1982, *J. Geophys. Res.*, *95*, 11,179–11,195.

Silver, P. G. (1996), Seismic anisotropy beneath the continents: Probing the depths of geology, *Annu. Rev. Earth Planet. Sci.*, *24*, 385–432.

Silver, P. G., and W. W. Chan (1988), Implications for continental structure and evolution from seismic anisotropy, *Nature*, *335*, 34–39.

Silver, P. G., and W. W. Chan (1991), Shear-wave splitting and subcontinental mantle deformation, *J. Geophys. Res.*, *96*, 16,429–16,454.

Silver, P. G., and W. E. Holt (2002), The mantle flow field beneath western North America, *Science*, *295*, 1054–1058.

Silver, P. G., and S. Kaneshima (1993), The APT89 seismic experiment: Shear-wave splitting results, *Geophys. Res. Lett.*, *20*, 1127–1130.

Silver, P. G., and M. K. Savage (1994), The interpretation of shear-wave splitting parameters in the presence of two anisotropic layers, *Geophys. J. Int.*, *119*, 949–963.

Silver, P. G., S. S. Gao, and K. H. Liu, and the Kaapvaal Seismic Group (2001), Mantle deformation beneath southern Africa, *Geophys. Res. Lett.*, *28*, 2493–2496.

Simiyu, S. M., and G. R. Keller (1997), An integrated analysis of lithospheric structure across the east African plateau based on gravity anomalies and recent seismic studies, *Tectonophysics*, *278*, 291–313.

Slack, P. D., and P. M. Davis, and the KRISP Teleseismic Working Group (1994), Attenuation and velocity of *P*-waves in the mantle beneath the east African rift, Kenya, *Tectonophysics*, *236*, 331–358.

Sleep, N. H., C. J. Ebinger, and J.-M. Kendall (2002), Deflection of mantle plume material by cratonic keels, in *The Early Earth: Physical, Chemical and Biological Development*, edited by C. M. R. Fowler, C. J. Ebinger, and C. J. Hawkesworth, *Geol. Soc. Spec. Publ. London*, *199*, 135–150.

Theunissen, K., J. Klerkx, A. Melnikov, and A. Mruma (1996), Mechanisms of inheritance of rift faulting in the western branch of the East African Rift, Tanzania, *Tectonics*, *15*, 776–790.

Tommasi, A. (1998), Forward modeling of the development of seismic anisotropy in the upper mantle, *Earth Planet. Sci. Lett.*, *160*, 1–13.

Tommasi, A., A. Vauchez, and R. Russo (1996), Seismic anisotropy in oceanic basins: Resistive drag of the sublithospheric mantle?, *Geophys. Res. Lett.*, *23*, 2991–2994.

Vauchez, A., G. Barruol, and A. Tommasi (1997), Why do continents break up parallel to ancient orogenic belts?, *Terra Nova*, *9*, 62–66.

Vauchez, A., G. Barruol, and A. Nicolas (1999), Comment on "*SKS* splitting beneath continental rift zones" by Gao et al., *J. Geophys. Res.*, *104*, 10,787–10,789.

Vinnik, L. P., L. I. Makeyeva, A. Milev, and A. Y. Usenko (1992), Global patterns of azimuthal anisotropy and deformations in the continental mantle, *Geophys. J. Int.*, *111*, 433447.

Walker, K. T., G. H. R. Bokelmann, and S. L. Klemperer (2001), Shear-wave splitting to test mantle deformation models around Hawaii, *Geophys. Res. Lett.*, *28*, 4319–4322.

Walker, K. T., G. H. R. Bokelmann, and S. L. Klemperer (2003), Reply to Shear-wave splitting to test mantle deformation models around Hawaii by Vinnik et al., *Geophys. Res. Lett.*, *30*(13), 1676, doi:10.1029/2002GL016712.

Weeraratne, D. S., D. W. Forsyth, K. M. Fischer, and A. A. Nyblade (2003), Evidence for an upper mantle plume beneath the Tanzanian craton from Rayleigh wave tomography, *J. Geophys. Res.*, *108*(B9), 2427, doi:10.1029/2002JB002273.

Wenk, H. R., K. Bennett, G. R. Canova, and A. Molinari (1991), Modeling plastic deformation of peridotite with the self-consistent theory, *J. Geophys. Res.*, *96*, 8337–8349.

Wessel, P., and W. H. F. Smith (1991), Free software helps map and display data, *Eos Trans. AGU*, *72*, 441, 444–445.

Wolfe, C. J., and P. G. Silver (1998), Seismic anisotropy of oceanic upper mantle: Shear-wave splitting methodologies and observations, *J. Geophys. Res.*, *103*, 749–771.

Wolfe, C. J., and S. C. Solomon (1998), Shear-wave splitting and implications for mantle flow beneath the MELT region of the East Pacific Rise, *Science*, *280*, 1230–1232.

Wookey, J., J.-M. Kendall, and G. Barruol (2002), Mid-mantle deformation inferred from seismic anisotropy, *Nature*, *415*, 777–780.

Wylegalla, K., G. Bock, J. Gossler, and W. Hanka, and the TOR Working Group (1999), Anisotropy across the Sorgenfrei-Tornquist Zone from shear wave splitting, *Tectonophysics*, *314*, 335–350.

Zhang, S., and S. Karato (1995), Lattice preferred orientation of olivine aggregates deformed in simple shear, *Nature*, *375*, 774–777.

G. H. R. Bokelmann, Laboratoire de Tectonophysique, Université de Montpellier II, Place Eugene Bataillon CC049 34095 Montpellier Cedex 05, France. (goetz.bokelmann@dstu.univ-montp2.fr)

S. L. Klemperer, Department of Geophysics, Stanford University, Stanford, CA 94305, USA. (sklemp@stanford.edu)

A. A. Nyblade, Department of Geosciences, Pennsylvania State University, University Park, PA 16802, USA. (andy@geosc.psu.edu)

T. J. Owens, Department of Geological Sciences, University of South Carolina, Columbia, SC 29201, USA. (owens@sc.edu)

K. T. Walker, Institute of Geophysics and Planetary Physics, Scripps Institution of Oceanography, University of California, San Diego, 9500 Gilman Avenue, MC 0225, La Jolla, CA 92093-0225, USA. (walker@ucsd.edu)

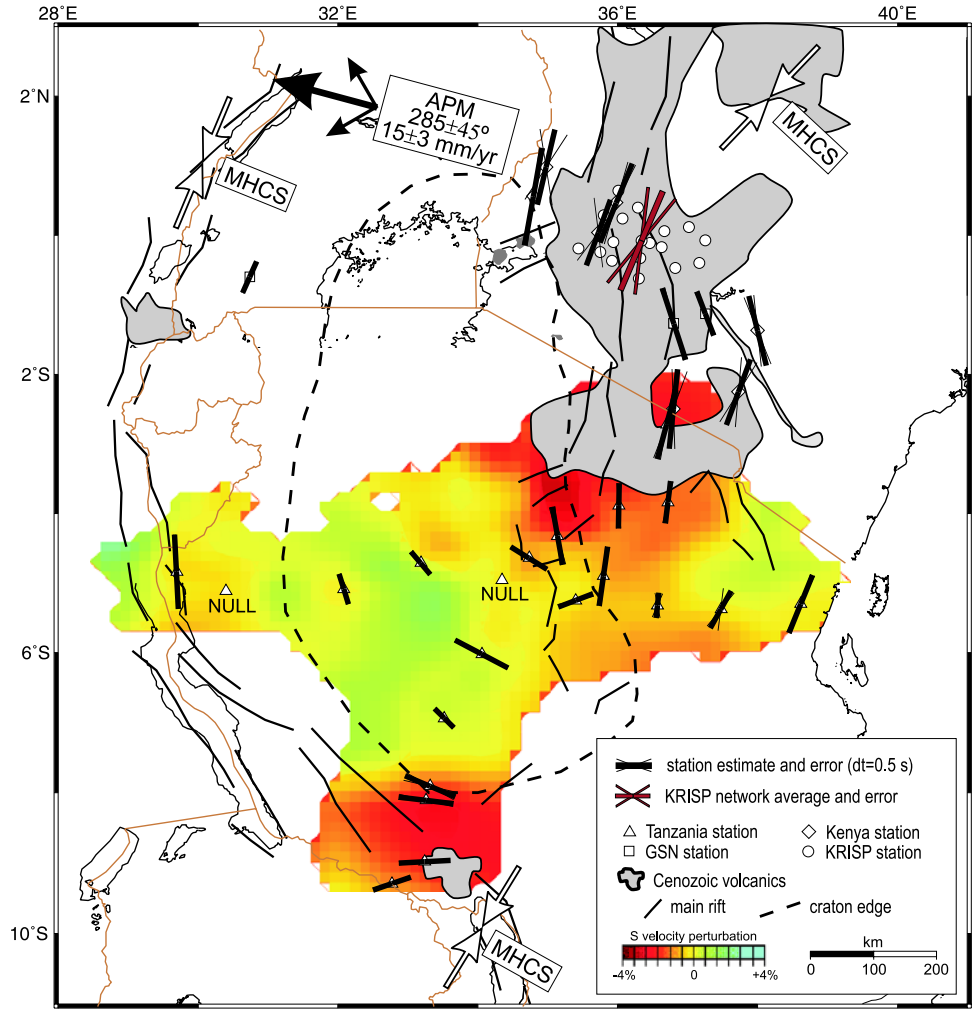

Figure 9. Single-layer horizontal-axis splitting models. Color indicates shear wave velocity tomographic slice at 200 km depth [*Ritsema et al.*, 1998]. Black arrow indicates the absolute plate motion direction [*Gripp and Gordon*, 2002]. White double arrows indicate the maximum horizontal compressive stress directions (MHCS) taken from regional averages of good-quality stress measurements (B. Mueller et al., The 2000 release of the World Stress Map 2000, available at http://www.world-stress-map.org). The thick black lines indicate the fast direction (ϕ), and their length is proportional to delay time. Thin black lines indicate the 2σ error bars for ϕ, which are too small to see for most stations.

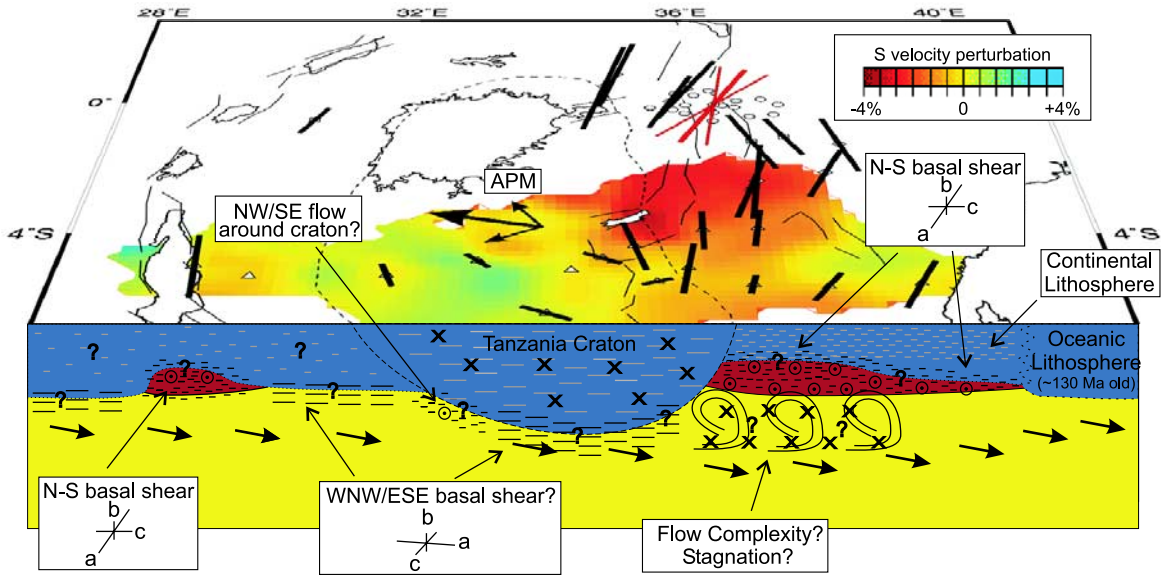

Figure 11. Cross section at 5°S showing possible sources of anisotropy that could explain splitting. Station splitting estimates are shown with delay time scaled to approximately correct for the three-dimensional view. A shear wave velocity tomographic image at 200-km depth is shown at the surface [*Ritsema et al.*, 1998]. The absolute plate motion (APM) is WNW [*Gripp and Gordon*, 2002]. Thin arrows in the asthenosphere (yellow) indicate the flow direction relative to the cratonic lithosphere (blue). Long dashes indicate olivine LPO with ~WNW/ESE fast *a* axes due to shear at the base of the keel (black) and fossilized from past orogenic events (gray). Shorter dashes indicate ~N/S fast *a* axes from plume flow (red) beneath thinned lithosphere and possible corner flow around the keel (black) and fossilized from prior orogenic events (gray). Crosses indicate additional anisotropy from previous orogenic events. Question marks indicate uncertain boundary locations and/or anisotropy. Dots with circles indicate flow is coming out of the page. The depth to the base of the craton is here defined by the 170-km depth to the center of the maximum negative shear wave velocity gradient [*Weeraratne et al.*, 2003].